1. Report No. ABC-UTC-UW 2016-4-2 -Final	2. Government Accession No.	3. Recipient's Catalog No.
4. Title and Subtitle Impact of Construction Eccentricity on Direct Pier-to-Pile Connections for Permanently Cased Shaft (CFST) Piles		5. Report Date January 2023 (FINAL REPORT DATE) 6. Performing Organization Code
7. Author(s) Spencer Lindsley Mu-Zi Zhao ORCID ID: 0000-0003-0974-1473 Dawn E. Lehman ORCID ID: 0000-0002-0823-1167 and Charles W. Roeder ORCID ID: 0000-0002-7160-291X		8. Performing Organization Report No.
9. Performing Organization Name and Address Department of Civil and Environmental Engineering University of Washington 201 More Hall Seat, WA 98195-2700		10. Work Unit No. (TRAIS) 11. Contract or Grant No. 69A3551747121
12. Sponsoring Organization Name and Address Accelerated Bridge Construction University Transportation Center Florida International University 10555 W. Flagler Street, EC 3680 Miami, FL 33174 US Department of Transportation Office of the Assistant Secretary for Research and Technology And Federal Highway Administration 1200 New Jersey Avenue, SE Washington, DC 201590		13. Type of Report and Period Covered Final Report (January 2021 – January 2022) 14. Sponsoring Agency Code
15. Supplementary Notes		
16. Abstract This is a second phase of a study investigation a direct connection between reinforced concrete (RC) piers and concrete filled steel tubes (CFSTs) piles or drilled shafts for accelerated construction of high-speed rail and other transportation systems. CFSTs are composite structural components consisting of a steel tube with concrete infill. They have greater strength and stiffness than typical RCs structural elements of comparable size, and permit accelerated construction because no internal reinforcement, shoring or formwork is required. CFST is suitable for piles and drilled shafts, but there has been little research on connections of RC columns to CFST piles and drilled shafts. This research is an experimental and analytical study of a new direct connection between these members. In this research, half-scale column-to-pile connections were tested to evaluate their inelastic behavior under seismic loading. Two specimens were tested with the primary focus on the nonlinear behavior and effect of long duration shaking and a supplemental rib to improve seismic performance. The transfer of the force and moment from the RC column to the CFST pile were closely monitored. The experiments showed that the addition of the internal rib improves the force and moment transfer. Long duration shaking is expected during large subduction earthquakes, but the increased number of inelastic deformation cycles did not adversely affect the performance of the connection. Nonlinear analyses were performed with the LSDyna computer program, and analytical results compared well with experimental observations. The test from this study and a prior research program were combined with analytical results to develop recommendations on the connection design.		
17. Key Words Connections, Concrete Filled Tubes, Pier Columns, Piles		18. Distribution Statement No restrictions.

19. Security Classification (of this report)	20. Security Classification (of this page)	21. No. of Pages	22. Price
Unclassified.	Unclassified.	94	

Form DOT F 1700.7 (8-72) Reproduction of completed page authorized

(this page is intentionally left blank)

Impact of Construction Eccentricity on Direct Pier-to-Pile Connections for Permanently Cased Shaft (CFST) Piles

Final Report
September 2022

Principal Investigators: Dawn E. Lehman and Charles W. Roeder
Department of Civil and Environmental Engineering
University of Washington

Authors

Spencer Lindsley, Mu-Zi Zhao, Dawn E. Lehman and Charles W. Roeder

Sponsored by
Accelerated Bridge Construction University Transportation Center

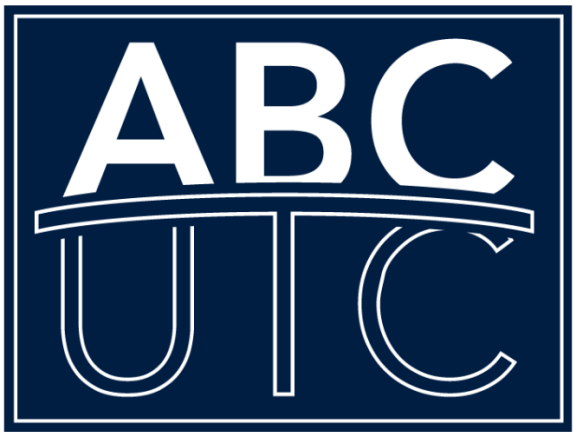

ACCELERATED BRIDGE CONSTRUCTION
UNIVERSITY TRANSPORTATION CENTER

A report from
Department of Civil and Environmental Engineering
University of Washington
More Hall, Box 352700
Seattle, WA 98103
Phone: 206-715-2108
https://www.ce.washington.edu

DISCLAIMER

The contents of this report reflect the views of the authors, who are responsible for the facts and the accuracy of the information presented herein. This document is disseminated in the interest of information exchange. The report is funded, partially or entirely, by a grant from the U.S. Department of Transportation's University Transportation Program. However, the U.S. Government assumes no liability for the contents or use.

TABLE OF CONTENTS

LIST OF FIGURES

LIST OF TABLES

ACKNOWLEDGEMENTS

This project was funded jointly by the Pacific Earthquake Engineering Research (PEER) Center and the Accelerated Bridge Construction University Transportation Center (ABC-UTC).

Chapter 1. INTRODUCTION

1.1 RESEARCH MOTIVATION

Concrete filled steel tubes (CFSTs) are a composite structural element that combines the compressive strength of concrete with the tensile strength and ductility of steel. They have been shown to provide greater strength and stiffness than traditional reinforced concrete (RC) elements of comparable size. CFSTs have significantly larger shear resistance than RC members of comparable size, and therefore CFSTs are very suitable for piles and drilled shafts in deep foundations at sites with liquefaction or lateral spreading of soil. CFSTs do not require formwork, shoring, or internal reinforcement, which accelerates construction and reduces cost.

In recent years, the seismic design forces on bridges have increased, which has led to increased demand on the structural resistance of bridge substructures. The use of CFSTs piles with RC columns provides the bridge with strength, stiffness, ductility, and energy dissipation for large lateral loads and deformations on the column and the pile. This combination also leads to accelerated construction and cost savings. However, connections between reinforced concrete (RC) columns and CFST piles and the mechanism of force and moment transfer between the two components are not well understood. This research is an initial study into a direct connection between RC piers Concrete filled steel tubes (CFSTs) piles or drilled shafts for accelerated construction of high-speed rail or other transportation systems. The study focused on understanding these connections, their transfer mechanisms, and how these mechanisms affect moment, axial, and shear forces on the connection behavior. An initial series of two tests were recently completed as an earlier phase of this research. This research builds upon that earlier study with additional experimental and nonlinear analytical research. The results of the earlier

research will be used extensively in this research study. Therefore, the earlier work will be briefly summarized but will not be repeated in any detail.

Prior analytical research, suggests that the bond between the RC column reinforcement and the concrete, and the bond between the tube and concrete are important elements of the transfer mechanism. The bond between the reinforcement and the concrete is dependent on the embedment depth of the reinforcement into the pile and the relative diameters of the column and pile. The bond between the tube and the concrete is affected by the type of steel tube used, with spirally welded tubes having shown to have more bond stress capacity than straight seam welded tubes. Adequate development length may be required to transfer the forces and moments of the RC column to the CFST pile. A steel rib welded to the interior of the tube may also aid in this force and moment transfer. This additional force transfer will be studied in this research project. In addition, the nonlinear analytical models will be developed, and the test results from this and the earlier project will be compared to results of nonlinear analyses performed using LS-Dyna, an FEA computer program. The finite element model can be calibrated and improved and the accuracy of the model estimated. This will allow the extension of this work through future nonlinear analysis studies.

1.2 RESEARCH OBJECTIVES

The initial experimental investigation evaluated the nonlinear performance of the proposed direct connection and examined the effect of the difference in diameter of the CFST pile and the RC pier column. To extend the results of this research this research study will:

- Experimentally investigate the inelastic behavior of a direct CFST pile to column connection with the additional mechanical bond mechanism.

- Experimentally investigate the inelastic response of a direct CFST pile to column connection under long-duration cyclic loading.
- Compare and validate the simulated finite-element model (FEM) results of the connection with the experimental measured results.

1.3 ORGANIZATION OF REPORT

This chapter introduces the subject. Chapter 2 provides a literature review and background to the experimental and analytical study. A detailed literature review of experimental research was provided in the prior study and so Chapter 2 will provide a very brief background of experimental work and a more detailed literature review of relevant analytical studies. Chapter 3 briefly summarizes results of the first two tests and provides a more detailed description of the additional tests. Chapter 4 describes the nonlinear analysis and compares the experimental results of the four tests to the analytical finite element model of Zhao. Chapter 5 summarizes the work, conclusions and recommendations.

Chapter 2. LITERATURE REVIEW AND TESTING BACKGROUND

2.1 FINITE ELEMENT ANALYSIS OF CFST PILE CONNECTION

2.1.1 *Analytical Investigation of a Direct Column-to-Cased Shaft Connection*

Zhao investigated the effects of different parameters on a RC Column to CFST, also called cased shaft, connection. The objective of the research was to determine the adequate embedment depth of the reinforcement if a supplemental mechanical bond was not included, as well as the requirements for placing the supplemental mechanical bond, rib, and the location of the reinforcing bars for required development length. The parameters of the study included: the embedment depth (l_d), the rib size (b_{nR}), the rib location (l_R), the reinforcing bar diameter, and the tube diameter (D).

The LS-Dyna finite element computer program was used to study the connection with the various parameters. The model used concrete constitutive models and bond-slip between both the tube and the concrete fill and the reinforcement and concrete. The concrete was modeled using a constant-stress solid element (LS-Dyna: ELFORM=1) with the Concrete Damage Plasticity Model (LS-Dyna: MAT273) for the constitutive model. The tensile and compressive damage parameters of the concrete are defined in the following equation:

$$\sigma = (1 - w_t)\sigma_t + (1 - w_c)\sigma_c$$

σ = effective stress tensor (ksi)
σ_t = tensile effective stress (ksi)
σ_c = compressive effective stress (ksi)
w_t = tensile damage parameter, varies from 0 (undamaged) to 1 (fully damaged)
w_c = compressive damage parameter, varies from 0 (undamaged) to 1 (fully damaged)

The steel tube was modeled using the Belytschko-Tsay shell element with the trilinear constitutive model, PIECEWISE_LINEAR_PLASTICITY (LS-Dyna: MAT024). The reinforcing bars were

modeled with the Hughes-Liu beam element with the combined kinematic model (LS-Dyna: MAT003). The reinforcement-concrete interface was modeled using the LS-Dyna function: BEAM_IN_SOLID, defining the bond-slip model proposed by Murcia-Delso (2015). The concrete fill-tube interface was modeled using the LS-Dyna contact element: AUTOMATIC_SURFACE_TO_SURFACE_TIEBREAK with Option = 9, which uses the cohesive material model MAT_COHESIVE_MIXED_MODE (LS-Dyna: MAT138). The interface between the tube rib and the concrete fill in the tube was modeled using the AUTOMATIC_SURFACE_TO_SURFACE contact with a coefficient of friction of 0.3. Figure 2.29 is the general schematic of the FE Model. The sizes of the elements were based on the diameter of their respective materials. The concrete element size was approximately d/15, with d being the diameter of the RC pier, or 1.33 in. The steel tube element size was approximately h_{CFST}/30 or 1.733 in. The steel rib element size was approximately D/30, with D being the diameter of the CFST, or 1 in. for the 30 in. diameter specimens and 1.6 in. for the 48 in. diameter specimens.

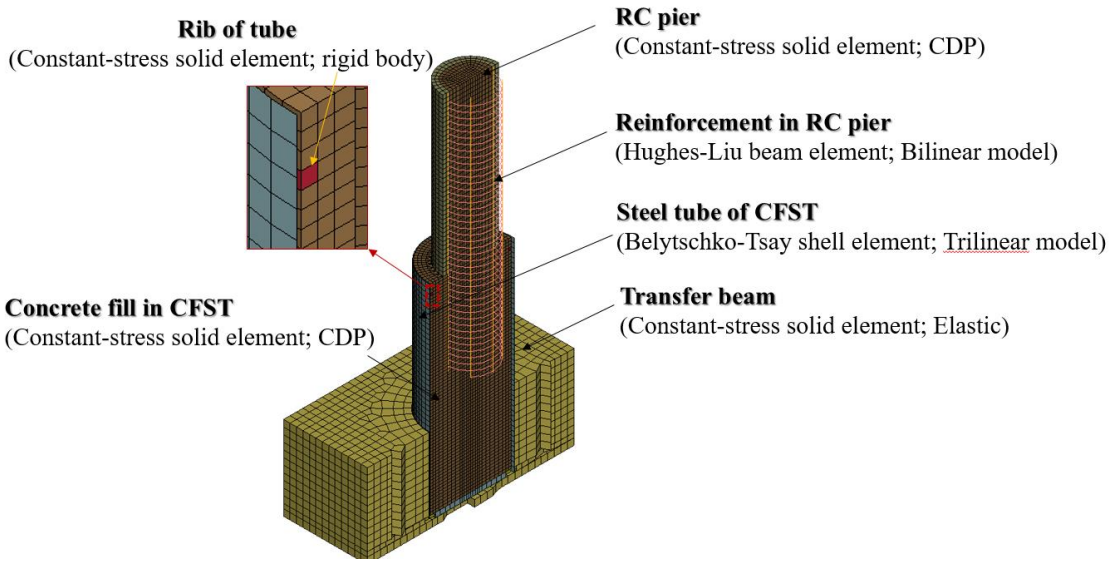

Figure 2.1. FE Model of RC Pier-to-Cased Shaft Connection

The model was verified by comparing the predicted and measured behavior to Xiao et al. (1998) and Han et al. (2016).

The parametric study showed the following results. Column longitudinal reinforcement embedment depths greater than 1.0D, one pile diameter, showed a full hysteretic response and sustained strength, while depths of 0.75D and 0.5D showed pinching in the response and loss of strength. The addition of a rib inside the pile leads to less concrete damage inside the pile and maximized the energy dissipation of the connection. The size of the reinforcing bar and location of the rib affected the strength degradation of the connection, with smaller reinforcement showing an improvement in strength degradation, which is due to the lower local bond demands. The larger tube diameter showed reduced concrete fill damage compared to the smaller tube diameter, and also had larger energy dissipation values.

The research produced by Zhao produced the following relevant conclusions:

- The embedment depth of the column reinforcing bars, for connections without a rib, must be equal to the greater of $l_{AASHTO,}$ AASHTO embedment length, and 1.0D
- The steel rib improves the structural performance of the connection and a rib size of b_{nR}=2/5 is recommended.
- The smaller reinforcing bar reduced the bond demand, concrete damage, and strength degradation of the connection.
- The rib should be located with $l_R \leq 0.3l_d$ to reduce concrete damage and strength deterioration.
- The larger diameter steel tube had less strength degradation and showed reduced damage to the concrete fill

Zhao's research was used as the basis for the specimen design of the experimental research described herein. Based on Zhao's findings, the important parameters to investigate were

embedment depth, pile diameter size, and the addition of the embedded steel rib inside the pile. Additional FEA is done on the proposed connections and described in further detail in Chapter 4.

2.2 BACKGROUND TO TESTING

In the prior research study, and comprehensive experimental literature review was provided. This review will not be repeated and the reader is referred to that document. Two test specimens were designed constructed and tested. One specimen, Specimen 30-21, had a 20 inch diameter RC pier column and 30 inch diameter CFST pile. The RC columns and the connections between the RC column and CFST pile are identical. The only difference is the diameter of the CFST pile. The tests showed that connections with rebar embedded into the CFST pile to the AASHTO required development length provided good performance. The larger diameter tube provide slightly performance. Some results of the first two tests will be briefly summarized in Chapter 3.

The two test specimens (Specimen 30-21R and Specimen 30-21LD) in this study will employ test specimens which are nominally identical to Specimen 30-21. Specimen 30-21LD is fully identical in construction, but Specimen 30-21R is identical except a rib is added to enhance bond stress transfer and development of composite action in the CFST pile. Specimen 20-30LD is truly identical but it is tested to a long duration seismic protocol, because subduction zone earthquakes are expected to have long duration seismic shaking and there increasing concern that this shaking may be more damaging to bridge systems. The construction, instrumentation and test procedures are identical for all specimens, and so the referred to the earlier document for these details.

While details are not provided. Figures 2.2 through 2.6 provide illustrations of the test specimens, instrumentation and test setup.

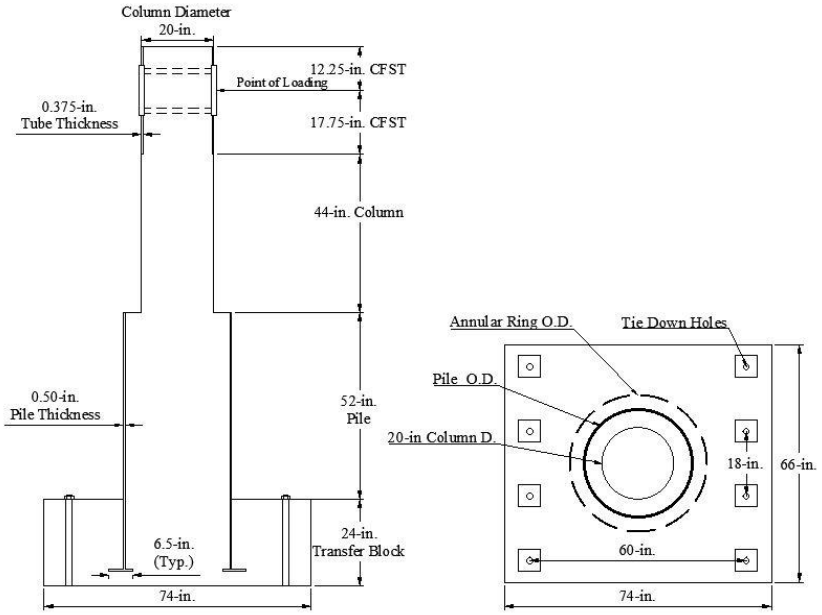

Figure 2.2. Specimen Layout and Dimensions a) Cross-section View b) Plan View

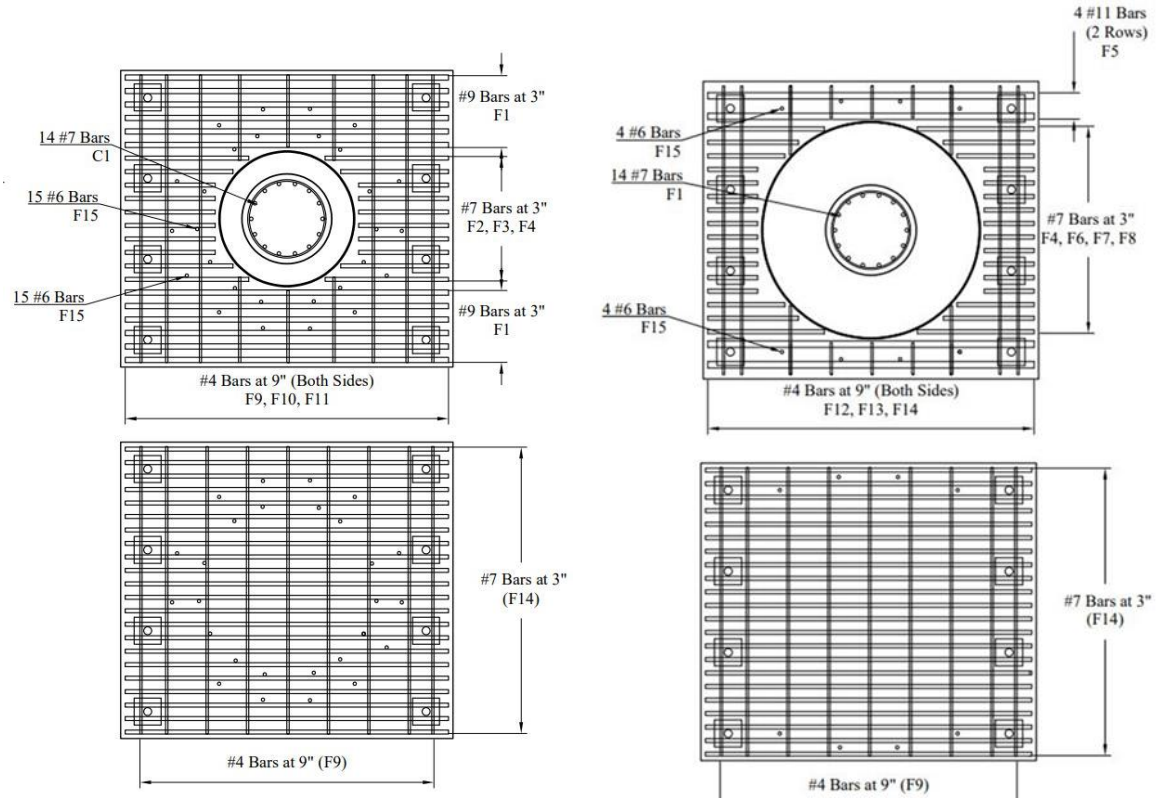

a) **b)**

Figure 2.3. Transfer Block Reinforcement a) Specimens 30-21, 30-21-R, and 30-21-LD and b) Specimen 48-21

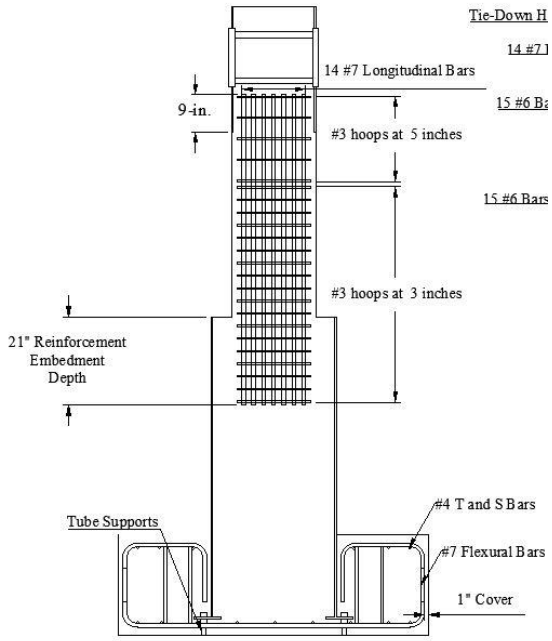

Figure 2.4. Typical Connection Reinforcement

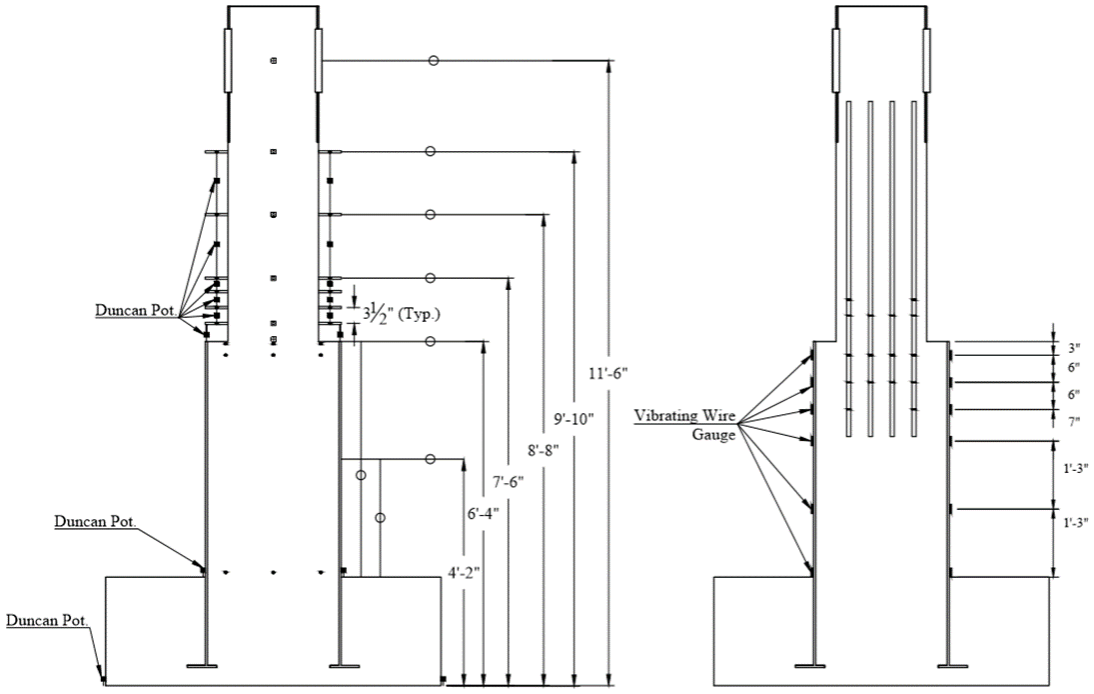

Figure 2.5. General Instrumentation Layout

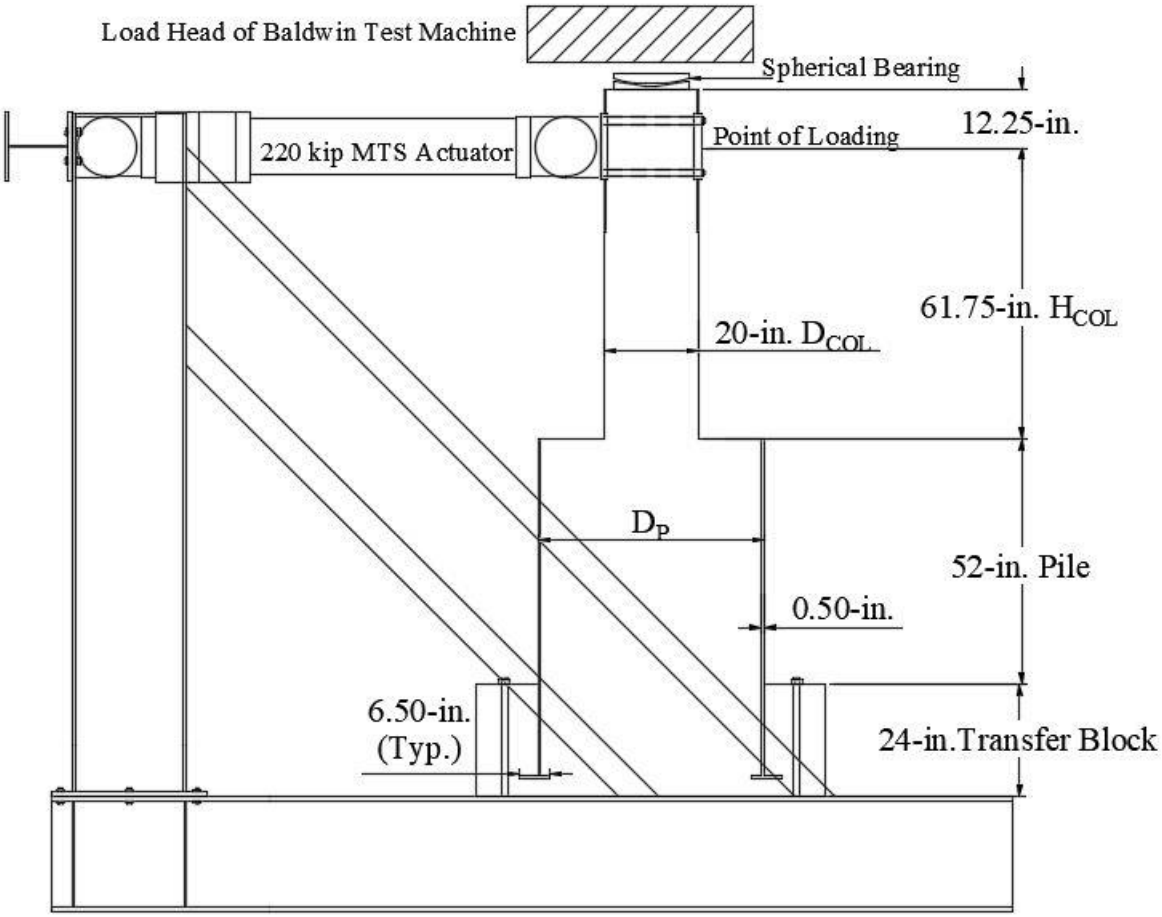

Figure 2.6. Experimental Setup Overview

Table 2.1. Specimen Test Matrix

Specimen Name	Tube Diameter (in.) [mm]	Tube Diameter/ Tube Thickness	Reinforcement Bar Size	Embedment Depth (in.) [mm]	Rib Size (in.) [mm]	Rib Embedment Depth (in.) [mm]
30-21*	30 [762]	60	#7	21 [533]	NA	NA
48-21	48 [1219]	96	#7	21 [533]	NA	NA
30-21-R	30 [762]	60	#7	21 [533]	2 [50.8]	2 [50.8]
30-21-LD	30 [762]	60	#7	21 [533]	NA	NA

2.2.1 *Specimen 30-21R*

Specimen 30-21R had a 2-inch wide by 0.5 in. thick rib was welded on the inside of the pile, 2 in. from the top of the pile using a fillet weld. As a result, the rib is embedded 2 inches into the concrete fill to enhance force and moment transfer as shown in Figure 2.7. This rib has been recommended as a method of improving seismic force transfer in CFST connections, but has never been experimentally evaluated.

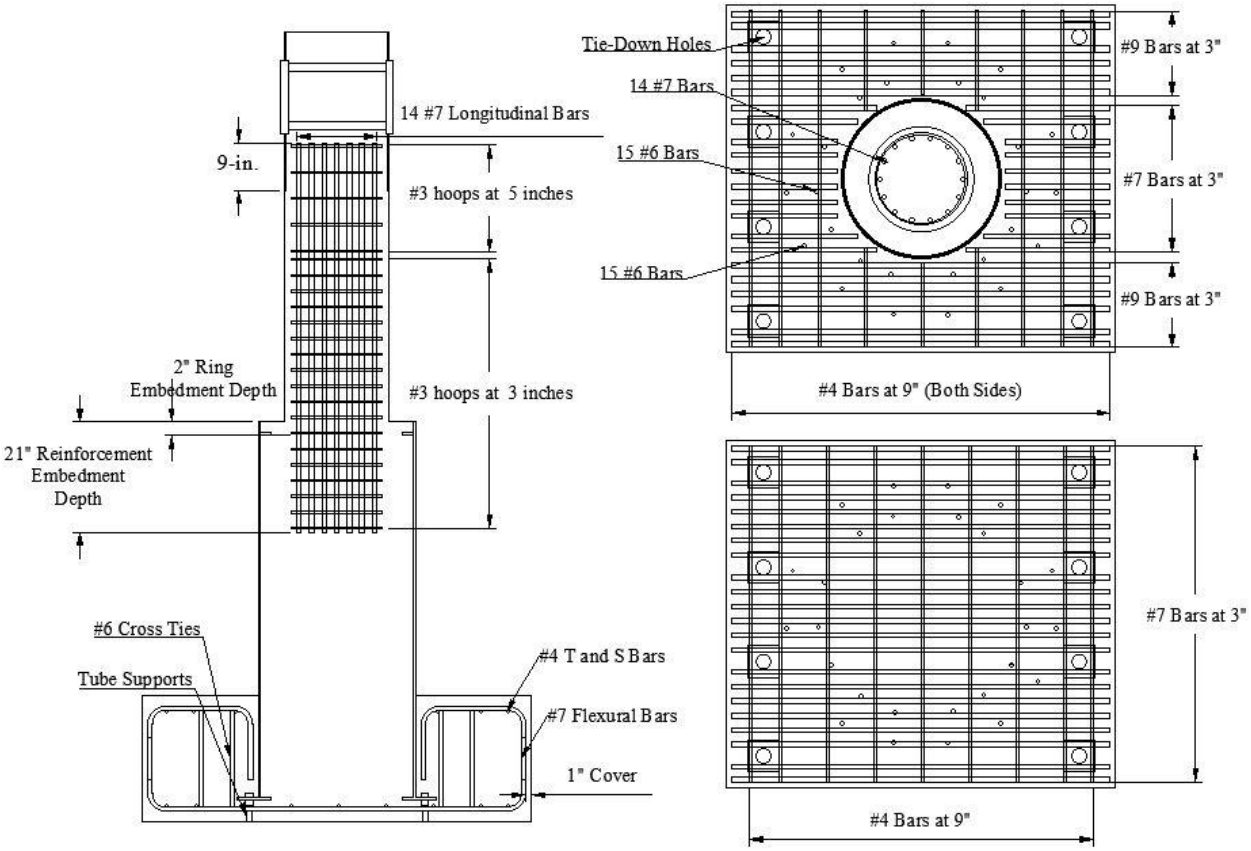

Figure 2.7. Specimen 30-21-R

Specimen 30-21-LD was tested under a long-duration displacement history. This displacement history was based on results from research by Kortum (2021), who investigated the impacts of a Cascadia subduction zone M9 earthquakes on bridges in Washington State for single degree of freedom (SDOF) idealized bridge columns.

Kortum modeled SDOF bridge columns under M9 ground motions. Assuming a bridge column located in Seattle, Washington, with a Bridge Strength Ratio, Fy/W, the bridges lateral strength divided by its weight, of 15%, bridge effective periods of 1.0 and 2.0s, and with a soil site classification of D3, 60 different hysteric displacement curves were modeled. Using the results of Specimens 30-21 and Kortum's hysteric curves, it was determined that a typical bridge column would undergo 6 cycles at a ductility when first spalling would occur, μ=2.7 or a column drift of 2%, one cycle at a ductility when full spalling would occur, μ=4.2 or a column drift of 3%, and 6 cycles at a ductility when bar buckling would occur, μ=5.7 or a column drift of 4%. The ductility is based on the results of Specimen 30-21 since it was identical to Specimen 30-21-LD. Based on these results, a testing displacement history was put together that consisted of 1 cycle at the expected yield displacement, 0.75 in., 6 cycles at 2.0 in, 1 cycle at 3.0 in., and then cycle to specimen failure, less than 50% of maximum strength at 4.0 in. This displacement history was slightly changed, as after 10 cycles at 6.5% drift the specimen had not failed, 2 cycles at 9.7% drift were run, as shown in Figure 2.8.

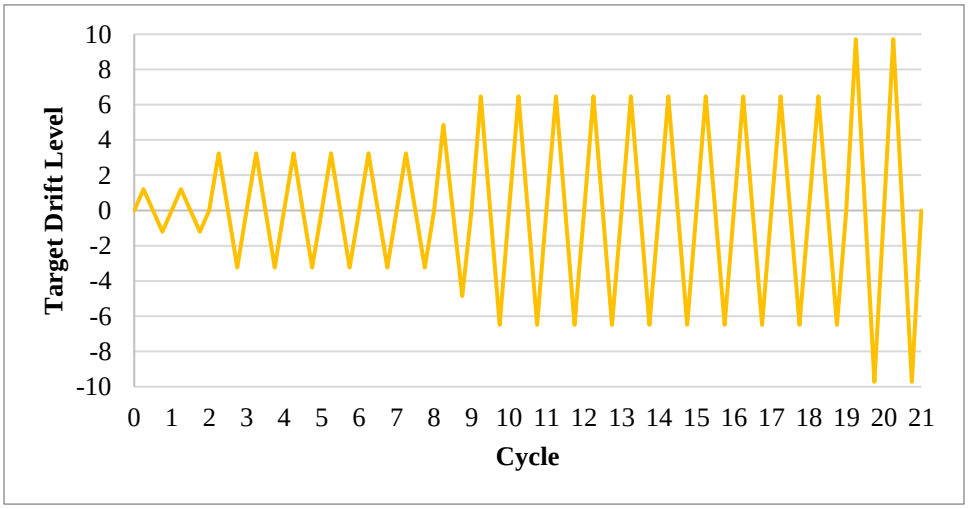

Figure 2.2. Specimen 30-21-LD Target Displacement History

Chapter 3. EXPERIMENTAL OBSERVATIONS AND RESULTS

3.1 INTRODUCTION

Experimental testing was conducted to assess the effects of pile diameter, reinforcement embedment depth, the addition of an embedded rib inside the pile, and displacement history on the cyclic, nonlinear performance CFST pile and RC column connections specimens. The first two specimens, Specimens 30-21 and 48-21, investigate the effect of pile diameter and embedment depth and were described in an earlier report. Since these results are used in the comparison to analytical results and the final conclusions of this report, a brief summary of those results are provided in Section 3.2.

The two remaining specimens, Specimen 30-21-R and Specimen 30-21-LD) are described in greater detail in Sections 3.3 and 3.4. The third specimen, Specimen 30-21-R, investigates the effect of the addition of the internal rib in the CFST pile. The fourth specimen, Specimen 30-21-LD, investigates the performance of the connection under long-duration cyclic loading.

3.2 BRIEF SUMMARY OF PRIOR TESTS

Figures 3.1 through 3.4 provide the force-deformation and moment-rotation behavior for Specimen 30-21. Figures 3.5 through 3.8 provide the force- deformation and moment-rotation behavior of Specimen 48-21.

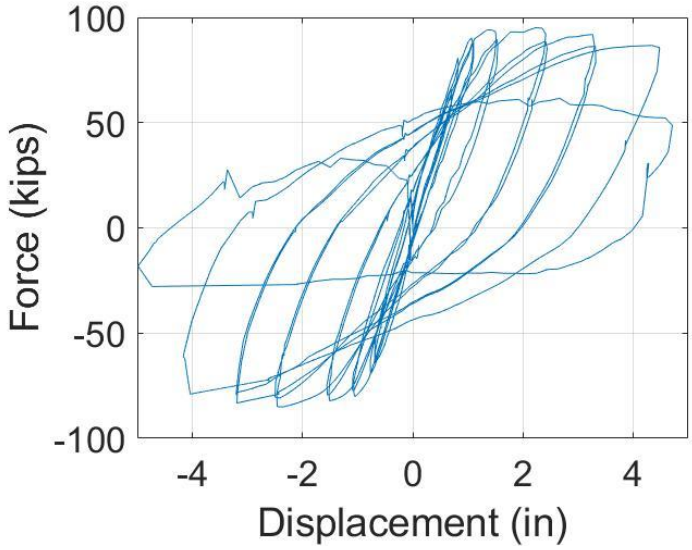

Figure 3.1. Specimen 30-21 Force-Displacement Curve with P-Δ Effects Removed

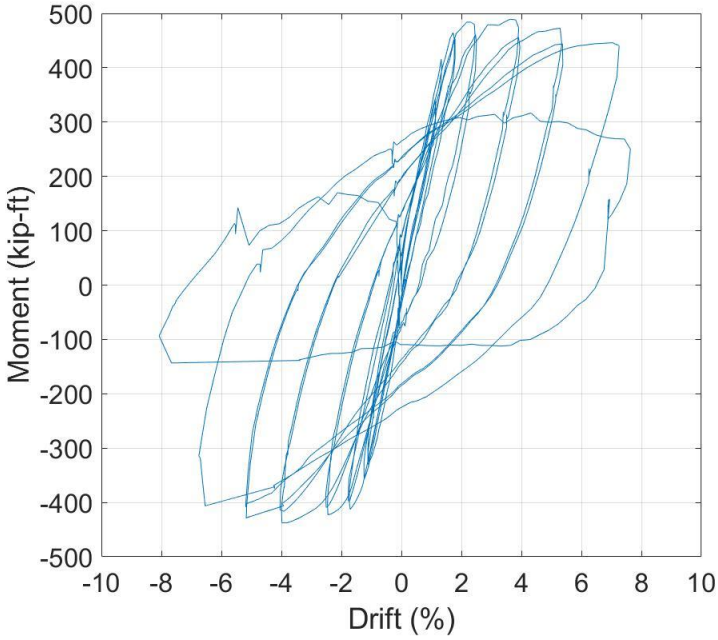

Figure 3.2. Specimen 30-21 Moment-Drift Curve with P-Δ Effects Removed

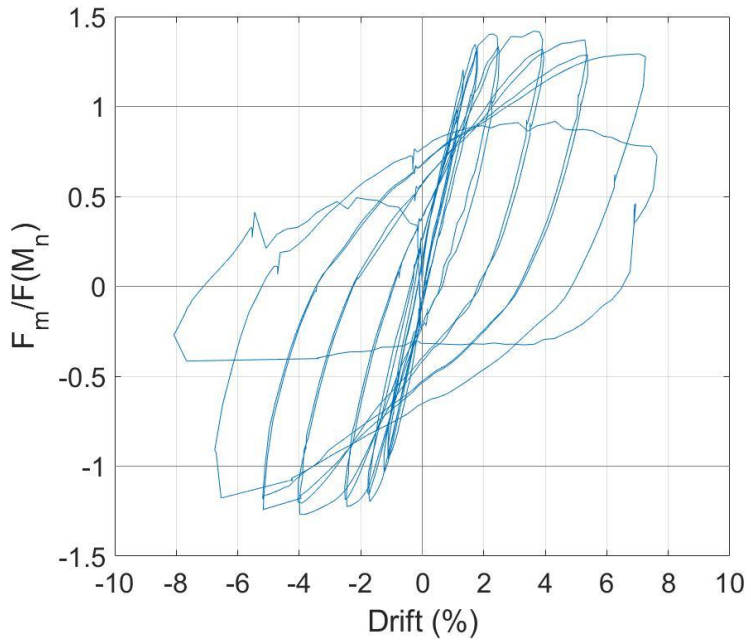

Figure 3.3. Specimen 30-21 Normalized by F_n Force-Drift Curve with P-Δ Effects Removed

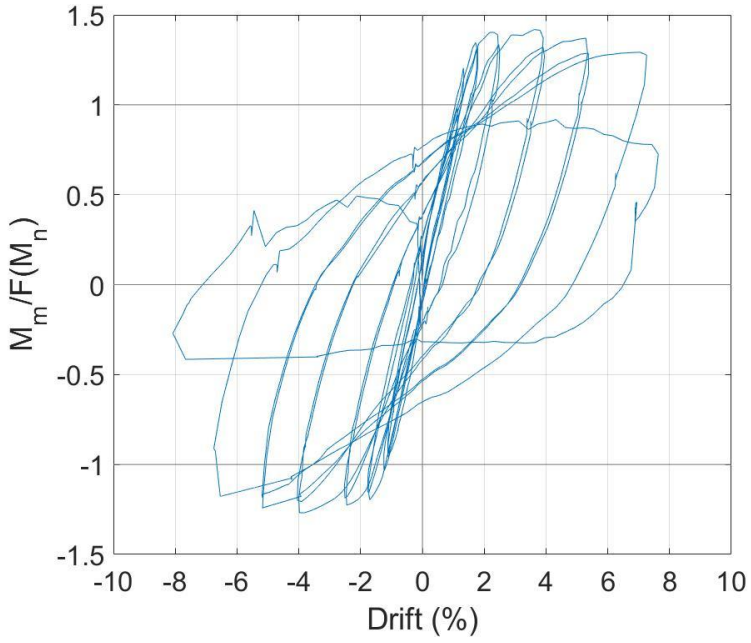

Figure 3.4. Specimen 30-21 Normalized by M_n Moment-Drift Curve with P-Δ Effects Removed

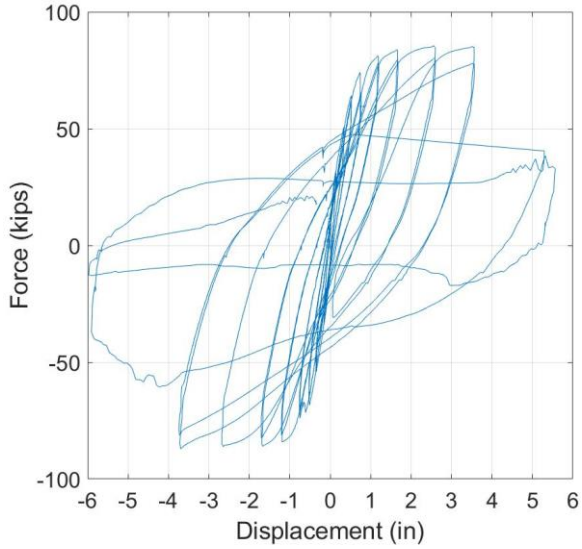

Figure 3.5. Specimen 48-21 Force-Displacement Curve

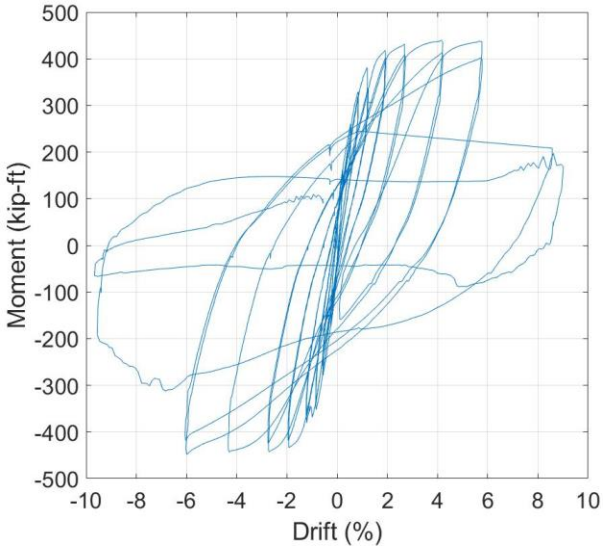

Figure 3.6. Specimen 48-21 Moment-Drift Curve with P-Δ Effects Removed

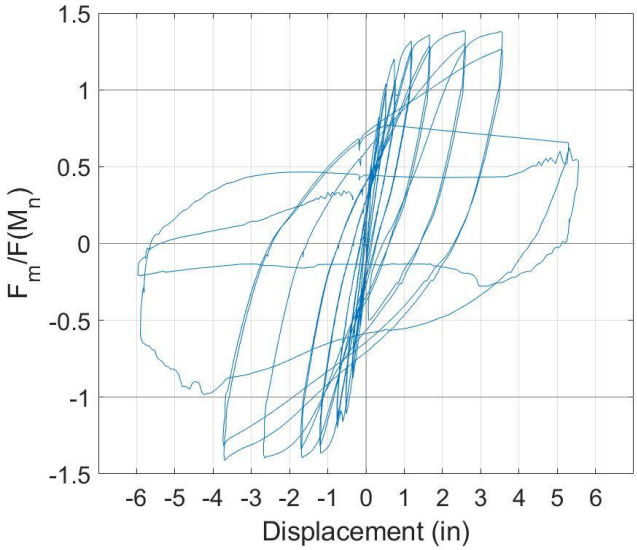

Figur3.7. Specimen 48-21 Force-Displacement Curve with P-Δ Effects Removed Normalized by F_n

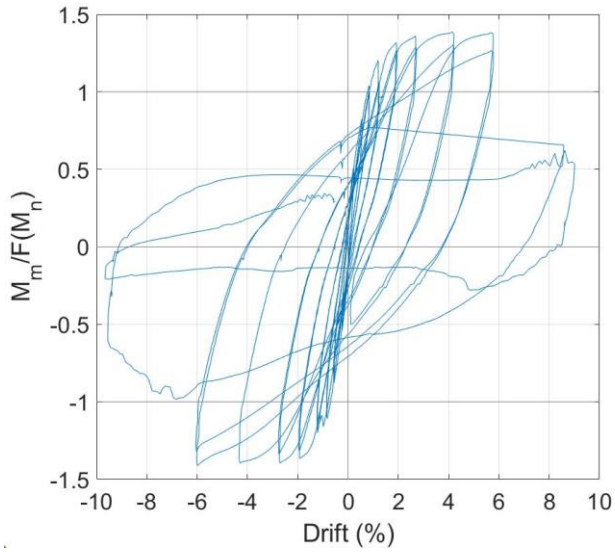

Figure 3.8. Specimen 48-21 Moment-Drift Curve with P-Δ Effects Removed Normalized by M_n

3.3 SPECIMEN 30-21-R

Specimen 30-21-R was tested on July 1st, 2021 in the Structural Research laboratory at the University of Washington. The test was performed 53 days after casting the transfer block and the pile, and 28 days after casting the column.

Specimen 30-21-R was identical with Specimen 30-21, except the tube now had a 2 in. wide steel rib welded inside 2 in. from the top of the tube.

Elastic cycles were run on this specimen, as the dry run for the specimen had a displacement of 0.1 in. The maximum measured resistances and corresponding imposed drifts of each cycle are found in Table 3.2. The normalized force-displacement and moment-drift hysteresis curves of the column and normalized versions are shown in Figures 3.9 to 3.12. The constant axial load applied to this specimen was 7.5% of the axial capacity of the column, 120 kips.

As shown in Figures 3.9 to 3.12 and Table 3.2, the largest moment, M_p, reached was 460.2 kip-ft or 1.43M_n, at -5.7% drift. The nominal moment, M_n, was 321.1 kip-ft for Specimen 30-21-R The lateral strength increased approximately 2% of M_p, or 10 kip-ft for each of the previous cycles at -2.4% and -4.0% drifts. The lateral strength decreases 4% of M_p on the first cycle at -9.3% drift, 10% M_p on the second cycle, 26% M_p on the thirds cycle, and then substantially drops 40% of M_p or 193 kip-ft with the last cycle, which reached the largest drift of -9.8%. The behavior is similar on the positive drift side as well.

Table 3.1. Maximum Resistances and Drifts in Each Cycle (30-21-R)

Target Drift	Cycle	Maximum Measured Resistance (kips)		Maximum Imposed Drift (%)	
		Tension	Compression	Tension	Compression
0.40%	1	26.2	23.0	-0.20	0.15
	2	26.3	26.9	-0.20	0.19
0.81%	3	39.0	40.6	-0.45	0.47
	4	39.4	41.4	-0.45	0.46
1.21%	5	52.0	50.6	-0.76	0.73
	6	54.4	57.1	-0.78	0.77
1.62%	7	67.8	69.6	-1.05	1.05
	8	64.1	67.7	-1.08	1.06
2.42%	9	79.8	81.0	-1.74	1.69
	10	78.0	80.1	-1.78	1.69
3.24%	11	83.3	87.4	-2.51	2.35
	12	81.4	73.3	-2.53	2.40
4.86%	13	88.7	88.2	-4.06	3.93
	14	78.6	82.3	-4.10	3.97
6.48%	15	89.4	83.9	-5.66	5.44
	16	81.1	80.9	-5.72	5.49
9.72%	17	85.0	81.8	-8.90	8.35
	18	76.4	79.4	-9.03	8.39
	19	53.3	66.0	-9.30	8.53
	20	15.8	18.1	-9.82	8.95

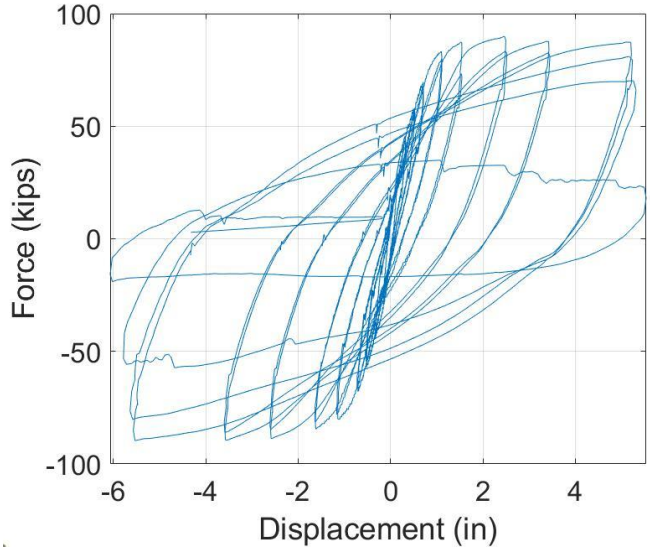

Figure 3.9. Specimen 30-21-R Force-Displacement Curve with P-Δ Effects Removed

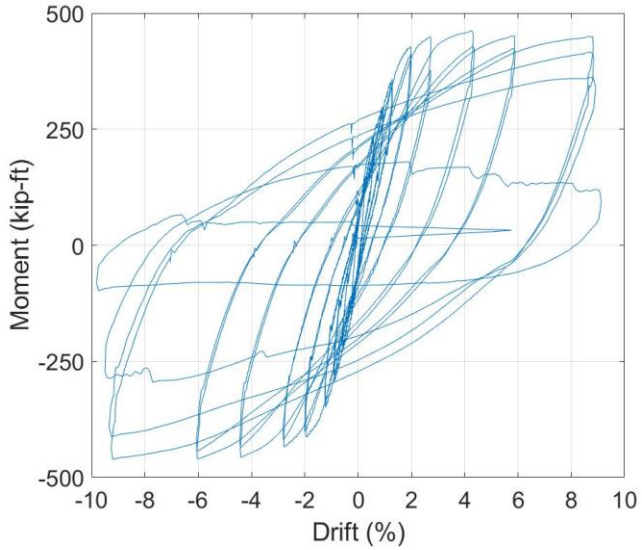

Figure 3.10. Specimen 30-21-R Moment-Drift Curve with P-Δ Effects Removed

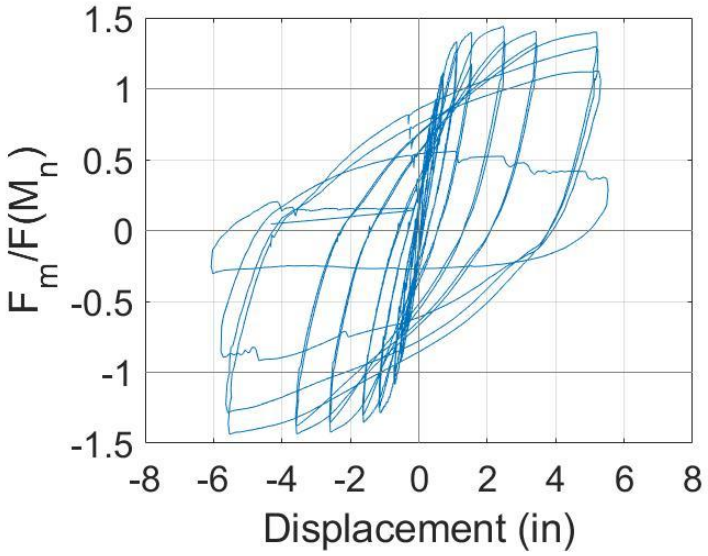

Figure 3.11. Specimen 30-21-R Force-Displacement Curve with P-Δ Effects Removed Normalized by F_N

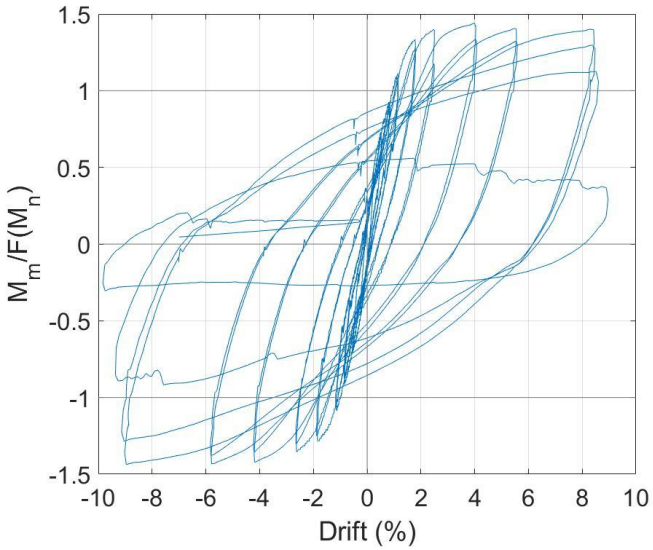

Figure 3.12. Specimen 30-21-R Moment-Drift Curve with P-Δ Effects Removed Normalized by M_n

For the initial cycles of the test, it was difficult to see initial cracks being formed. This is due to the type of latex paint used on the column. For the other specimens, normal drywall paint was used, which made it easier to see the cracks form. Beyond this difficulty to see the initial cracking, the use of latex paint did not affect the behavior of the column.

Table 3.3 shows the width and location of the maximum and residual cracks measured for each drift level.

Table 3.2. Maximum Measured Crack Widths and Locations for Each Cycle (30-21-R)

Drift Level	Maximum Crack		Residual Cracks	
	Width (mm)	Location	Width (mm)	Location
0.2%	NA	NA	NA	NA
0.5%	0.1	7 in. above base	NA	NA
0.8%	0.3	8 in. above base	NA	NA
1.1%	0.6	7 in. above base	NA	NA
1.8%	1.0	7 in. above base	0.4	6 in. above base
2.5%	1.5	7 in. above base	1.0	6 in. above base
4.1%	2+	7 in. above base	0.8	11 in. above base
5.5%	2+	7 in. above base	1.5	11 in. above base
9.0+%	2+	7 in. above base	Spall	Base of Column

3.3.1 *Low Drift Cycles (0-2.0% Drift)*

For drift cycles of approximately 0.2%, the lateral load ranged from -0.4 to 0.4 (-26.2 to 26.9 kips) times the nominal force, F_n, which for this specimen was 62.4 kips. As mentioned before, due to the latex paint no visible cracks were formed during this cycle. Strains measured during the peak displacement of the cycle were well within the reinforcement strain of 0.0023 in/in.

At drift cycles of 0.5%, the lateral load ranged from -0.6 to $0.7F_n$ (-39.4 to 41.4 kips), an increase of $0.2F_n$ from the previous cycle. A 0.1 mm wide horizontal crack formed $0.3D_{COL}$ (6 in.) from the base of the column on the northern face, shown in Figure 3.13. No residual cracks were measured at zero force displacements.

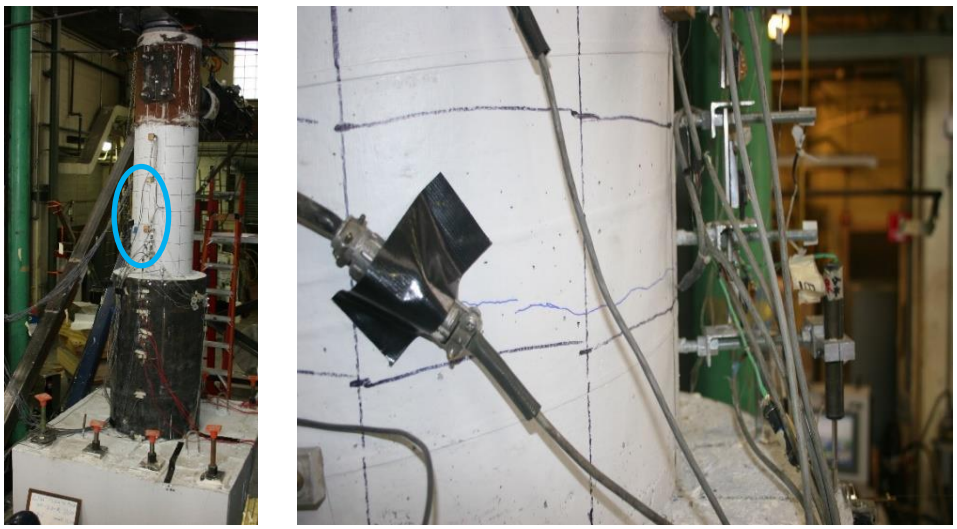

Figure 3.13. Specimen 30-21-R Horizontal Crack on Northern Column Face at 0.5% Drift

For this drift level, none of the longitudinal reinforcement strain measurements at peak displacement reached the approximate yield strain of 0.0023 in/in, with the largest strain, 0.0015 in/in, of these cycles, occurring on the $0.3D_{COL}$ location on the S Bar.

At 0.8% drift, the lateral load ranged from -0.9 to $0.9F_n$ (-54.4 to 57.1 kips), an increase of $0.3F_n$ from the previous cycle. Horizontal cracks on the northern and southern faces formed

roughly every 0.25D_{COL} (5 in.) going up the height of the column, which can be shown in Figure 3.14, with the maximum width of the cracks being 0.3 mm, which occurred 0.3D_{COL} (6 in.) from the base on the North side of the column.

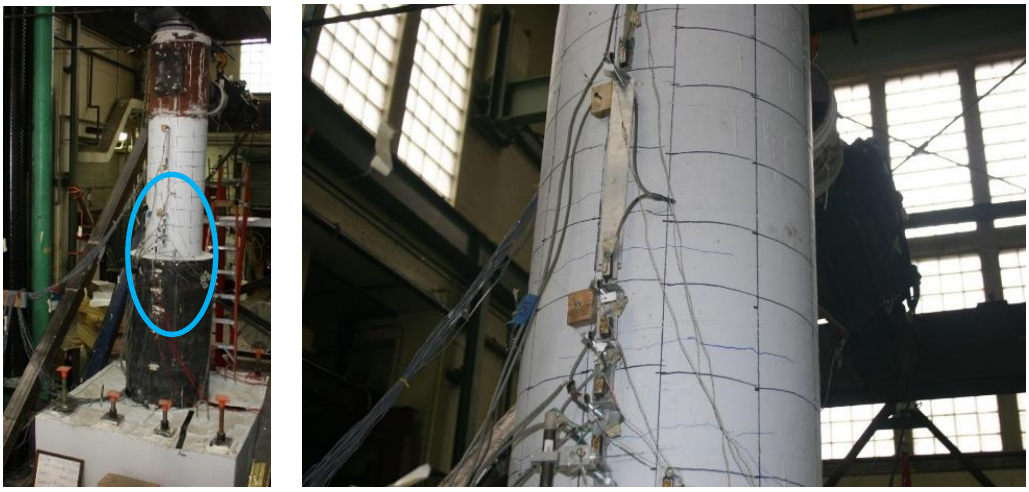

Figure 3.14. Specimen 30-21-R Horizontal Cracks on Northern Column Face at 0.8% Drift

During the first cycle at 0.8% drift, the column reinforcement strain exceeded the yield strain of 0.0023 in/in at 0.3D_{COL} on the S bar, during the peak displacement as shown in Figure 3.16.

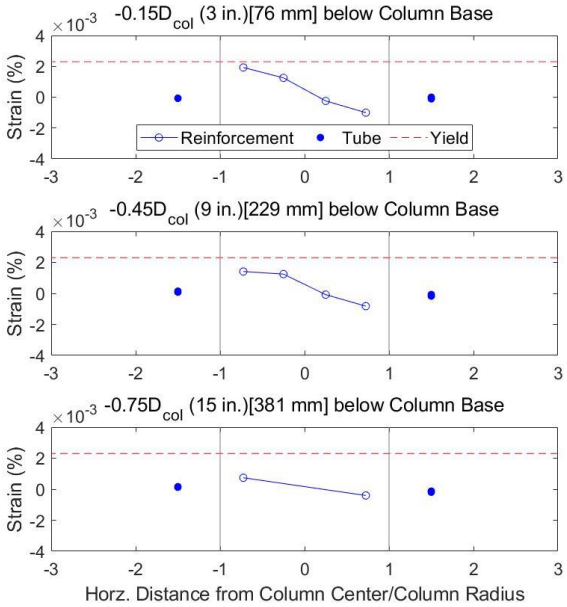

Figure 3.15. Specimen 30-21-R Strain Distribution at 0.8% Drift

At approximately 1.1% drift, the lateral load ranged from -1.1 to $1.1F_n$ (-67.8 to 69.6 kips), an increase of $0.2F_n$ from the previous cycle. The already formed horizontal cracks continued to lengthen, with the largest crack having a maximum width of 0.6 mm as shown in Figure 3.16. Additional horizontal cracks formed $1.5D_{COL}$ (30 in.) up on the column as well. During zero force, no residual cracks were visible, and the already formed cracks closed up.

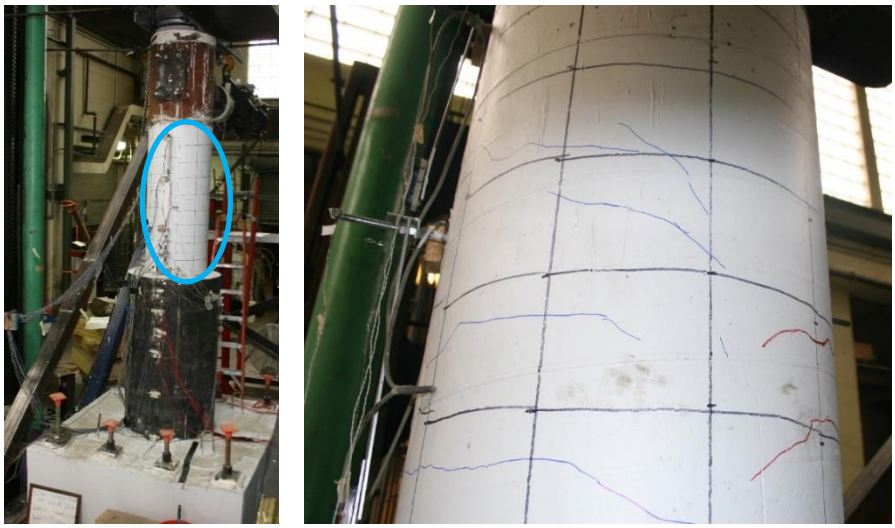

Figure 3.16. Specimen 30-21-R Horizontal Cracks at 1.1% Drift

The strains measured at the peak displacement of this cycle, exceeded the yield strain for all locations from $-0.45D_{COL}$ to $0.45D_{COL}$, shown in Figure 3.17. The strains reached 0.004 in/in, at $0.3D_{COL}$ on the S bar. The locations at $-0.75D_{COL}$ did not reach the reinforcement yield strain.

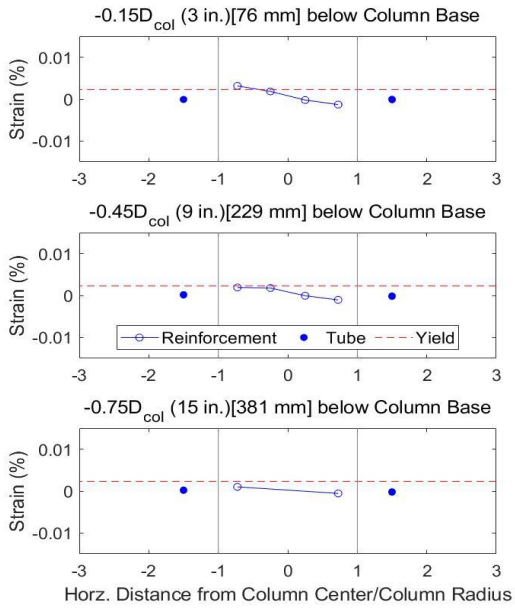

Figure 3.17. Specimen 30-21-R Strain Distribution at 1.1% Drift

At drift displacements of 1.75%, the lateral loads ranged from -1.3 to 1.3F_n (-79.8 to 81.0 kips) an increase of 0.1F_n from the previous cycle. The measured cracks widened noticeably to a maximum width of 1.0 mm. The largest cracks were located on the northern and southern faces, both 6 in. from the base of the column, as shown in Figure 3.18. During the zero-force displacements at this cycle, the southern cracks were not visible at all, but the northern cracks 6 in. from the base of the column were visible and had a width of 0.4 mm.

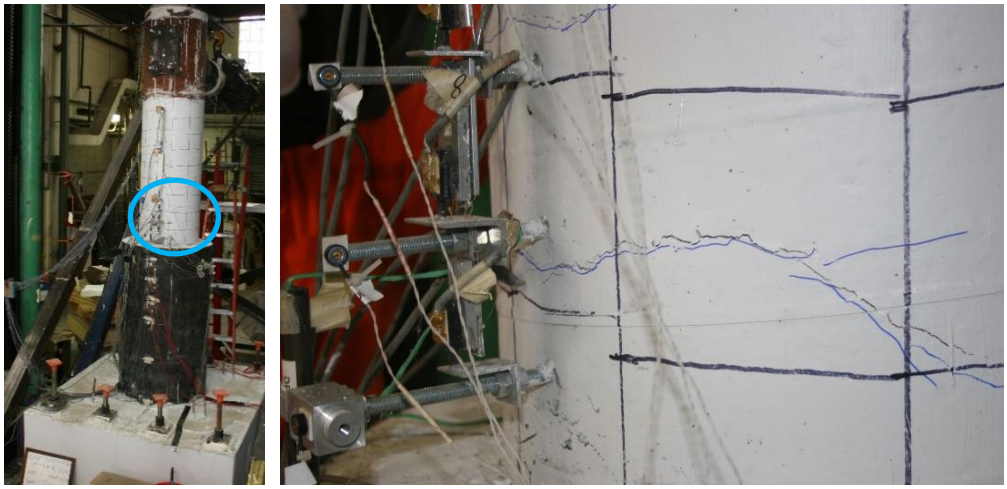

Figure 3.18. Specimen 30-21-R Column Northern Face crack at 1.75% Drift

Similar to the previous cycle, the strains measured at the peak displacement of this cycle, exceeded the yield strain for all locations from -0.45D_{COL} to 0.45$D_{COL,}$ shown in Figure 3.19. The largest strain was 0.0091 in/in, which occurred at 0.3D_{COL} on the S bar.

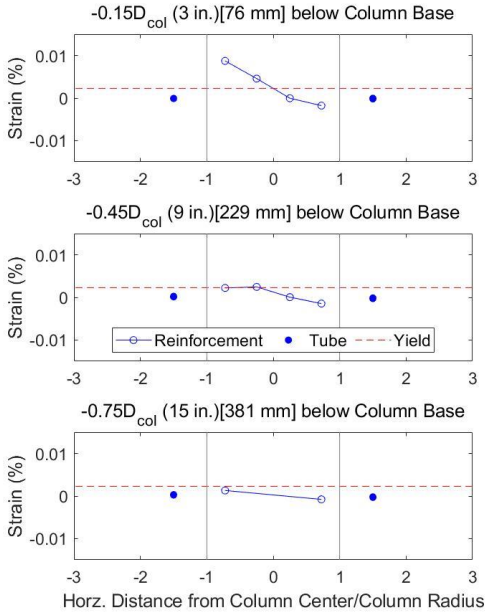

Figure 3.19. Specimen 30-21-R Strain Distribution at 1.75% Drift

3.3.2 *Moderate Drift Cycles (2.0-4.0% Drift)*

On the following cycle, at 2.4% drift, the lateral load ranged from -1.3 to 1.4F_n (-83.3 to 87.4 kips), an increase of 0.1F_n from the previous cycle. The horizontal cracks continued to expand, with the widest crack occurring 0.3D_{COL} (6 in.) up from the base of the northern side of the column with a width of 1.5 mm. During this cycle, a small spalled region formed at the base of the northern face, which can be shown in Figure 3.20.

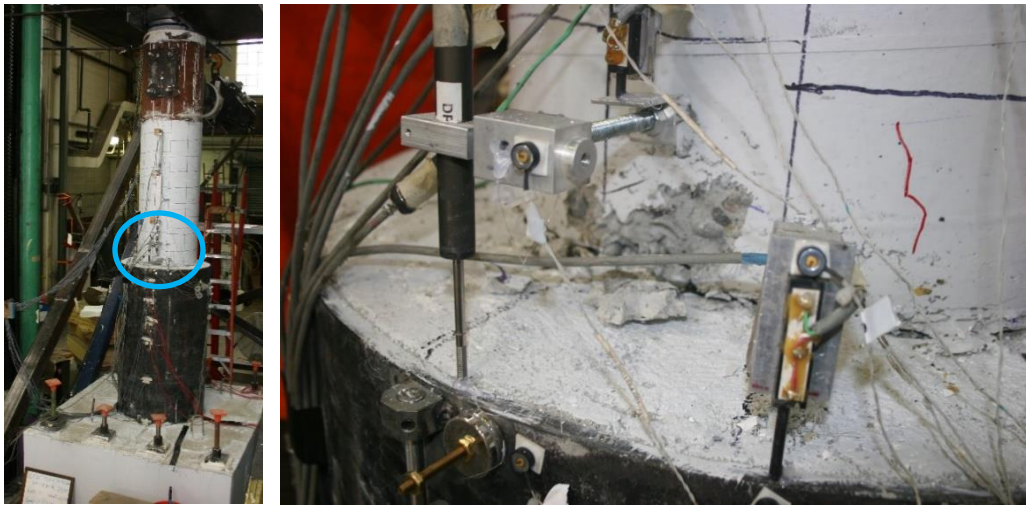

Figure 3.20. Specimen 30-21-R Spalled Region at Base of North Face of Column at 2.4% Drift

As with the previous cycle, the strains measured at the peak displacement of this cycle, exceeded the yield strain for all N and S bar locations, except -0.75D_{COL}. The strains reached up to 0.014 in/in, which occurred on the S bar at 0.3D_{COL}.

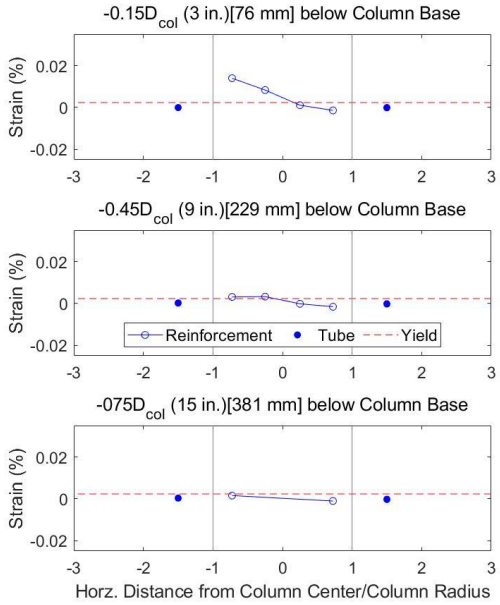

Figure 3.21. Specimen 30-21-R Strain Distribution at 2.4% Drift

At drift cycles of 4.0%, the lateral load ranged from -1.4 to 1.4F_n (-88.7 to 88.2 kips), which is approximately equivalent to the previous cycle. It was during this cycle the column sustained its

peak positive moment, $1.4M_n$ or 456.5 kip-ft when removing P-Δ effects. The spalling region increased to a 10 in. by 7 in. area and the horizontal cracks at the base of the column increased to a maximum width of greater than 2 mm. The transverse column reinforcement was exposed as shown in Figure 3.22. The crack between the base of the column and the top of the pile expanded and had a depth of 2 in., as shown in Figure 3.24.

Figure 3.22. Specimen 30-21-R Exposed Transverse Reinforcement at 4.0% Drift

Figure 3.23. Specimen 30-21-R 2 in. Deep Crack at Northern Base of Column at 4.0% Drift

As with the previous cycle, the strains measured at the peak displacement of this cycle, exceeded the yield strain for all N and S bar locations, except for the N bar and S bar locations -0.75D_{COL}, as shown in Figure 3.24. The strains reached up to 0.028 in/in, which occurred on the S bar at 0.3D_{COL}.

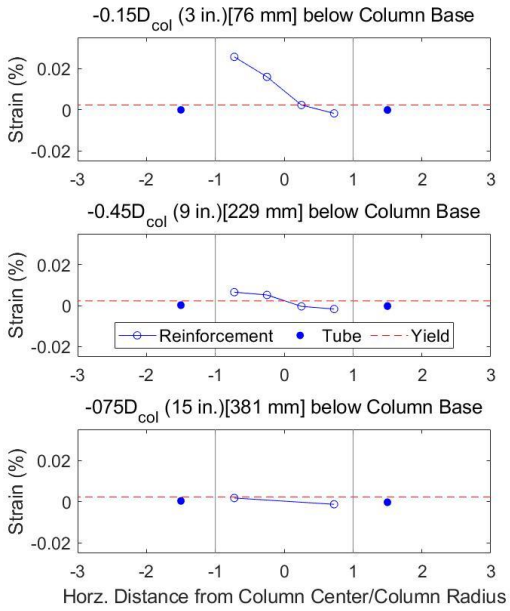

Figure 3.24. Specimen 30-21-R Strain Distribution at 4.0% Drift

3.3.3 *Large Drift Cycles (Greater than 4.0% Drift)*

At drift cycles of 5.5%, the lateral load ranged from -1.4 to 1.3 F_n (-89.4 to 83.9 kips) approximately equivalent to the last cycle. At this drift level, in the negative direction, the maximum negative moment of 1.4M_n or 460.2 kip-ft. The spalled region and the crack at the column base increased in size and exposed the longitudinal reinforcement on the northern face, shown in Figure 3.25. The spalled region now had an area of 20 in. by 8 in. on the north side and 10 in. by 5 in. on the south side. From this point on the cracks were too large to be measured, but all continued to increase in size and quantity.

Figure 3.25. Specimen 30-21-R Exposed Northern Longitudinal Reinforcement at 5.5% Drift

At 8.9% drift for the first cycle, the lateral load ranged from -1.4 to $1.3F_n$ (-85.0 to 81.8 kips) a decrease less than $0.1F_n$ from the previous cycle. The spalled region on both faces continued to increase with multiple longitudinal and transverse reinforcement being exposed. One of the longitudinal bars on the southern side buckled. There was also significant concrete crushing and the longitudinal bars buckled in both compression and tension, this can be shown in Figure 3.26. The spalling was so widespread that horizontal cracks could not be measured.

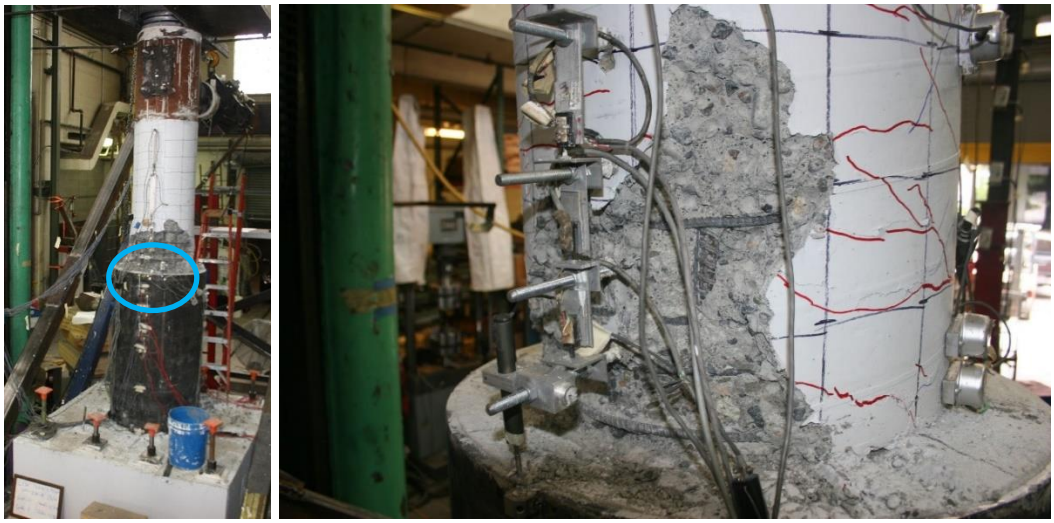

Figure 3.26. Specimen 30-21-R South Face Buckled Longitudinal Reinforcement Bars at 8.9% Drift

On the second cycle at 8.9% drift, the lateral load ranged from -1.3 to $1.3F_n$ (-81.1 to 80.9 kips), a decrease less than $0.1F_n$ from the previous cycle. The longitudinal reinforcement buckled in both compression and tension as shown in Figure 3.27. The spalled region on the northern side increased to an area of 25 in. by 15 in. and an area of 20 in. by 15 in. on the southern side.

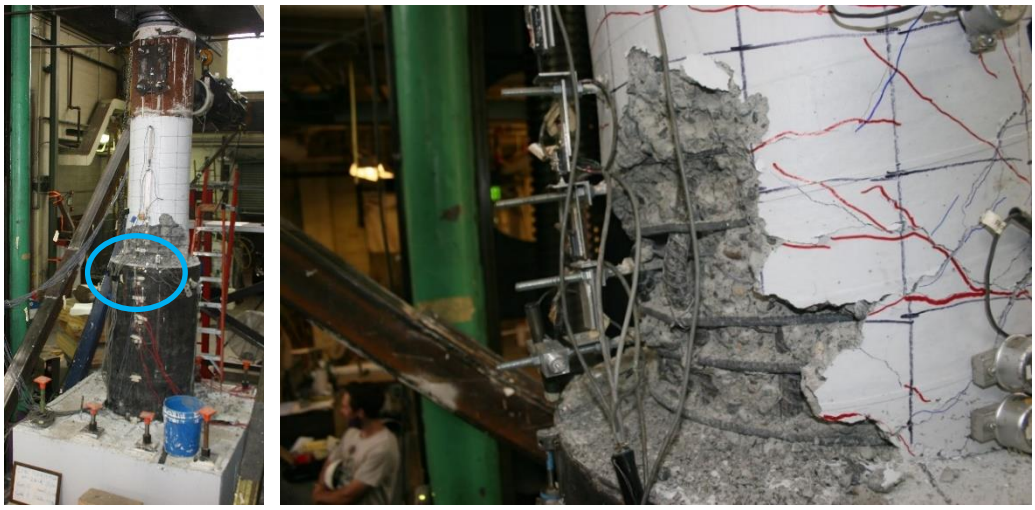

Figure 3.27. Specimen 30-21-R Buckled Reinforcement at 8.9% Drift

During the previous tests, loading was terminated after two cycles at 8.9% drift, however, since Specimen 30-21-R had not shown significant strength loss two more full cycles were run at 9.3% drift until the 50% strength loss had occurred. During the third cycle, a column drift of 9.3% was reched. The maximum lateral load was $1.1F_n$ (66 kips), a decrease in strength of $0.2F_n$ from the previous cycle or $0.4F_n$ from the peak strength of $1.4F_n$ (89.4 kips). During this cycle, concrete around the entire base of the column spalled off and the reinforcement continued to buckle, as shown in Figure 3.28.

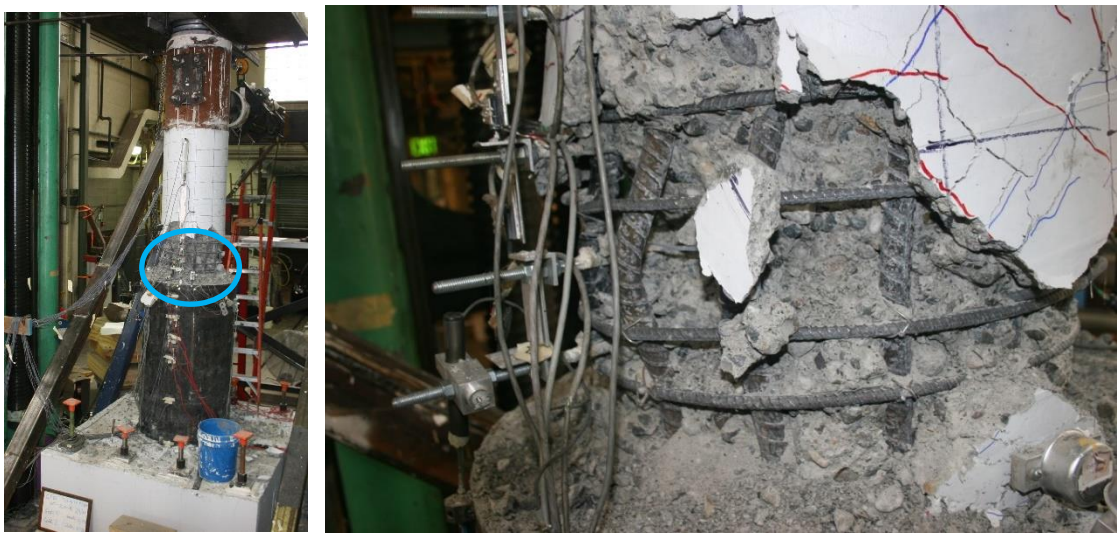

Figure 3.28. Specimen 30-21-R Base of Column at 9.3% Drift

Loading was terminated after 9.8% drift, with all bars buckled and the bottom $0.25D_{COL}$ (5 in.) of the column concrete separated from the rest of the pile. Similar to previous specimens, during the last cycle, the concrete at the base of the column seemed to explode out, as did the transverse reinforcement at the base too. The final state of the specimen can be shown in Figure 3.29. The lateral load on the last cycle was $0.3F_n$ (18.1 kips), a decrease of $0.8F_n$ (48 kips) from the previous cycle, or a decrease of $1.1F_n$ (71.1 kips) from the peak force.

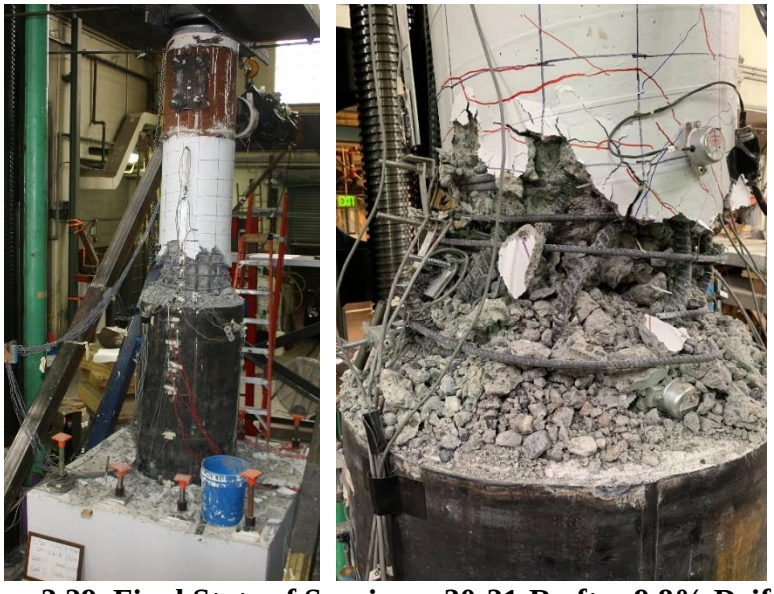

Figure 3.29. Final State of Specimen 30-21-R after 9.8% Drift

Throughout all load cycles, the pile and transfer block showed no visible damage. The largest measured strain in the pile was 0.008 in/in, which occurred 52 in. below the top of the tube, during the 4.0% drift cycles. No cracks formed anywhere on the transfer block. There was no noticeable slip between the pile concrete in comparison to the edge of the tube at any point of the test. The Duncan potentiometer measuring the slip had a maximum uplift of 0.003 in. As shown in Figure 3.30, the top of the pile concrete appears largely undamaged. Unlike Specimens 30-21 and 48-21, no radial cracks formed on the top of the pile concrete.

Figure 3.30. Top of Specimen 30-21-R Pile with Column Removed

The day after the test, when working on removing the specimen from the testing rig, it was noticed that the most extreme southern longitudinal reinforcing bar had fractured overnight. No applied loads had occurred between now and the end of testing, but the fracture was caused by the weight of the column resting overnight. The fractured bar is shown in Figure 3.31.

Figure 3.31. Specimen 30-21-R Fractured Longitudinal Reinforcement

3.4 SPECIMEN 30-21-LD

Specimen 30-21-LD was tested on July 13th, 2021 in the Structural Research laboratory at the University of Washington. The test was performed 40 days after casting the transfer block and the pile, and 33 days after casting the column. The design of Specimen 30-21-LD was identical with Specimen 30-21, with the difference being the testing displacement history described in Chapter 2.

Elastic cycles were run on this specimen, as the dry run for the specimen had a displacement of 0.1 in. The maximum measured resistances and corresponding imposed drifts of each cycle are found in Table 3.4. The force-displacement and moment-drift hysteresis curve and the normalized curves of the column are shown in Figures 3.32 to 3.35. The constant axial load applied to this specimen was 7.5% of the axial capacity of the column, 160 kips.

Table 3.3. Maximum Resistances and Drifts in Each Cycle (30-21-LD)

Target Drift	Cycle	Maximum Measured Resistance (kips)		Maximum Imposed Drift (%)	
		Tension	Compression	Tension	Compression
1.21%	1	50.0	49.4	0.68	0.64
	2	54.4	52.1	0.69	0.75
3.24%	3	91.4	93.8	2.31	2.38
	4	88.4	88.1	2.37	2.38
	5	84.7	84.9	2.29	2.4
	6	84.6	84.0	2.38	2.41
	7	84.1	73.5	2.33	2.4
	8	84.7	76.9	2.37	2.41
4.86%	9	93.7	92.9	3.88	3.81
6.48%	10	98.9	90.0	5.77	5.36
	11	91.0	80.0	5.82	5.12
	12	92.8	79.0	5.8	5.15
	13	81.6	78.5	5.83	5.18
	14	87.3	76.3	5.88	5.19
	15	86.9	72.1	5.9	5.2
	16	79.3	74.5	5.89	5.23
	17	79.1	72.5	2.94	5.24
	18	81.0	70.8	5.98	5.26
	19	66.8	64.2	6.01	5.3
9.72%	20	52.4	54.8	9.43	8.33
	21	24.5	27.1	9.86	8.64

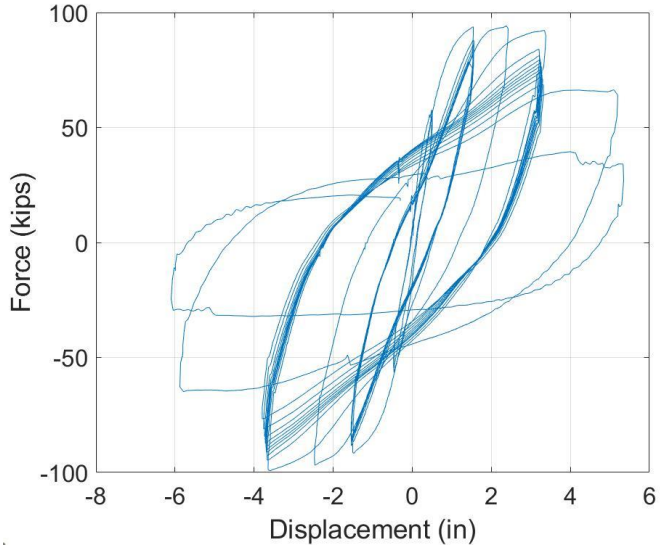

Figure 3.32. Specimen 30-21-LD Force-Displacement Curve with P-Δ Effects Removed

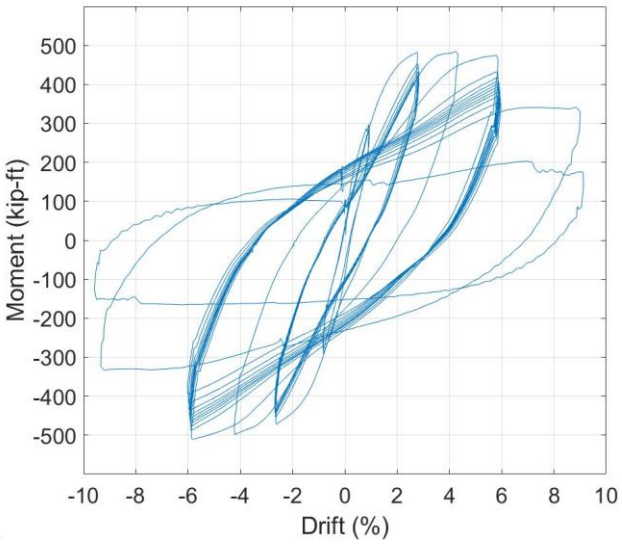

Figure 3.33. Specimen 30-21-LD Moment-Drift Curve with P-Δ Effects Removed

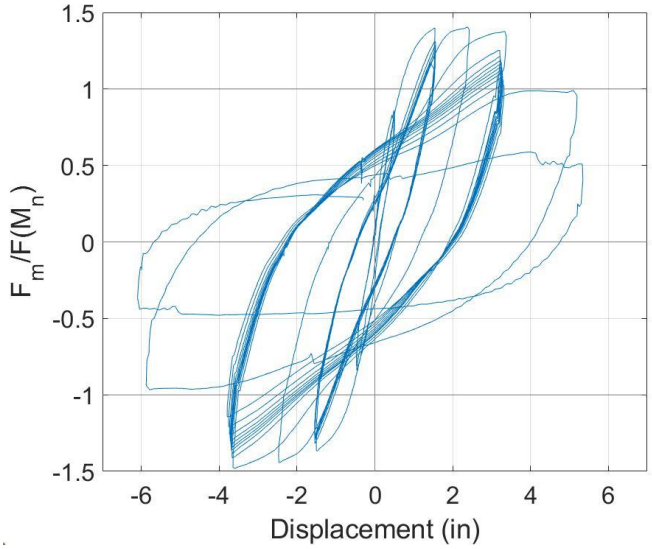

Figure 3.34. Specimen 30-21-LD Force-Displacement Curve with P-Δ Effects Removed Normalized by F_n

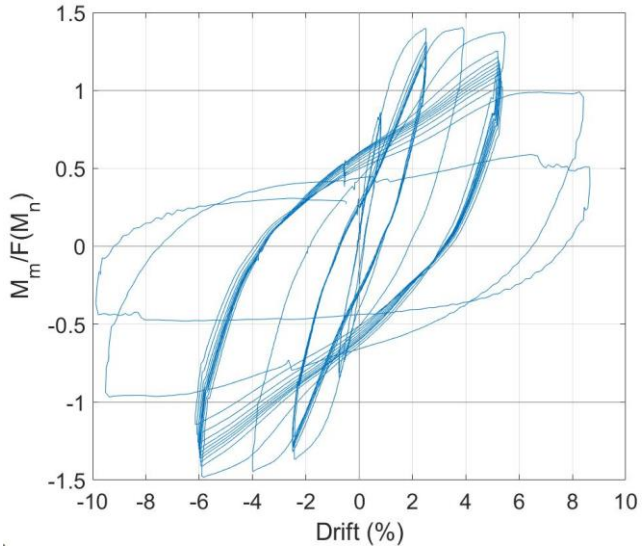

Figure 3.35. Specimen 30-21-LD Moment-Drift Curve with P-Δ Effects Removed Normalized by M_n

As shown in Table 3.4 and Figures 3.32-3.35, the largest moment, M_p, reached was 508.7 kip-ft or 1.47 M_n, at -5.8% drift. The nominal moment, M_n, was 345 kip-ft for Specimen 30-21-LD. It can be seen that the lateral resistance was approximately equal for the previous initial cycles at 2.4% and 3.9% drifts. The lateral resistance then degraded roughly 4% of M_p or 20 kip-ft with each following cycle at 5.5% drift. It then degrades roughly 20% of M_p or 100 kip-ft with each

cycle at 9.0% drift until it fails at a max drift of 9.9%. The behavior is similar in the negative drift direction as well The peak moment does line up with the peak lateral resistance when accounting for P-Δ delta effects, similar to Specimen 30-21.

Table 3.5 shows the width and location of the maximum and residual cracks measured for each drift level.

Table 3.4. Maximum Measured Crack Widths and Locations for Drift Level (30-21-LD)

Drift Level	Maximum Crack		Residual Cracks	
	Width (mm)	Location	Width (mm)	Location
0.7%	0.5	Base of Column	0.1	Base of Column
2.3%	2.4	Base of Column	2.0	Base of Column
3.8%	5.0	Base of Column	3.5	Base of Column
5.5%	Spall	Base of Column	Spall	Base of Column
9.0%+	Spall	Base of Column	Spall	Base of Column

3.4.1 *Low Drift Cycles (0-2.0% Drift)*

At 0.7% drift, the lateral load ranged from -0.8 to 0.8 times the nominal force, F_n, of 67.0 kips (-54.4 to 52.1 kips). Horizontal cracks on the northern and southern faces formed roughly every $0.25D_{COL}$ (5 in.) going up the height of the column, with the maximum width of the cracks being 0.5 mm, which occurred $0.25D_{COL}$ (5 in.) from the base on both the North and South sides. Cracks also formed around the perimeter of the tube, which can be shown in Figure 3.36.

Figure 3.36 Specimen 30-21-LD Cracks at Edge of the Pile at 0.7% Drift

The strains measured at the peak displacement came very close but did not exceed the reinforcement yield strain of 0.0023 in./in. as shown in Figure 3.37. The largest strain measured was 0.0017 in./in., which occurred at -0.15D_{COL} on the N bar.

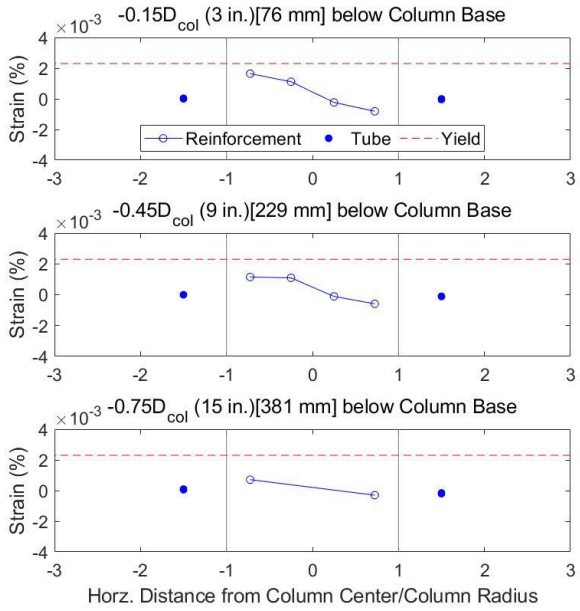

Figure 3.37. Specimen 30-21-LD Strain Distribution at 0.7% Drift

3.4.2 *Moderate Drift Cycles (2.0-4.0% Drift)*

After the first cycle at approximately 2.4% drift, the lateral load ranged from -1.4 to 1.4F_n (-91.4 to 93.8 kips) an increase of 0.6F_n from the previous cycle. New cracks continued to form and already formed horizontal cracks continued to lengthen. The largest measured crack width was 1.3 mm, located at the Southern base of the column. Radial cracks formed around the column, from the edge of the tube to the base of the column. The first spalling also occurred at the base of the column on the northern face, which can be shown in Figure 3.38.

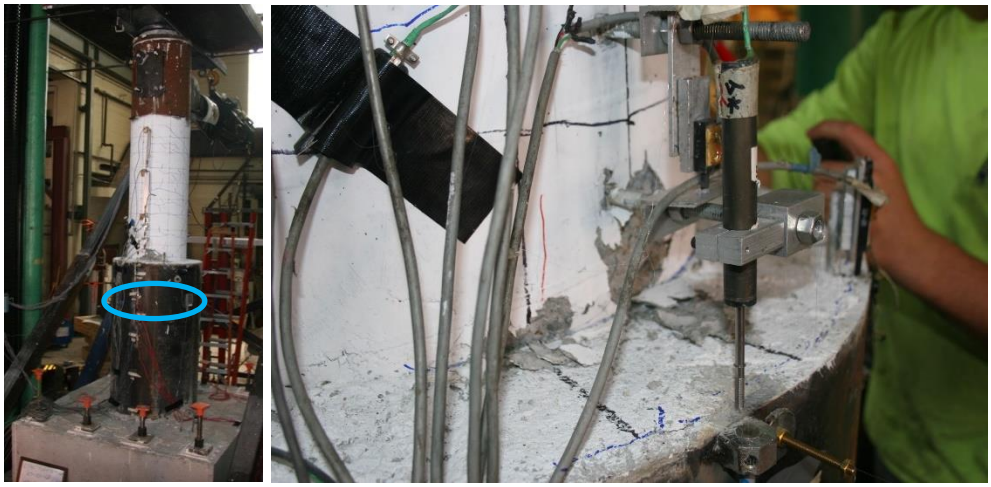

Figure 3.38. Specimen 30-21-LD 1st Spalled Region on Northern Column Face at 2.4% Drift

The reinforcement strain measured at the peak displacement on the N bar exceeded the yield strain of 0.0023 in./in. at $0.45D_{COL}$ and the other strain gauge located above. It is worth noting that while it was during this cycle the reinforcement yielded, this is not the yield displacement of the column, and nor is it an accurate representation of when the reinforcement should yield either. As shown with the other specimens, the reinforcement is closer to yielding around 0.8% drift.

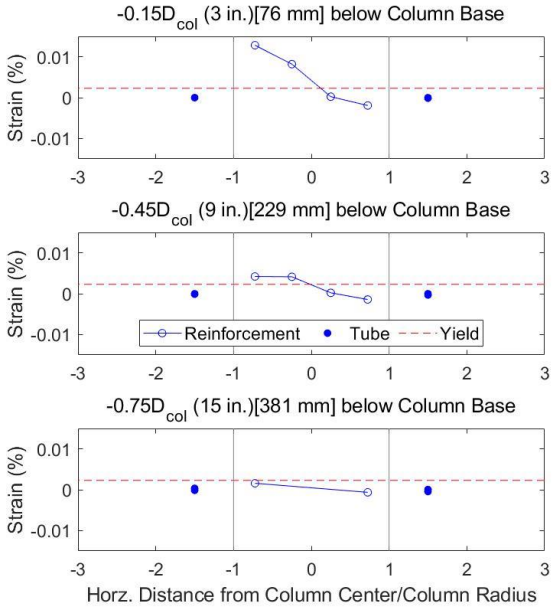

Figure 3.39. Specimen 30-21-LD Strain Distribution at 2.4% Drift

As cycles 3-6, at 2.4% drift, continued, four constant observations were noticed. The lateral load range for these cycles was -1.3 to $1.3F_n$ (-84.7 to 84.9 kips) a slight decrease from the first cycle at 2.4% drift. The horizontal cracks at the base of the column continued to widen to a width of 2.0 mm. The initial spalling at the base of the northern face of the column continued to increase in area and depth. The strains measured during these cycles were similar, with all strain gauge locations ranging from $-0.45D_{COL}$ to $0.45D_{COL}$ measured a strain greater than the reinforcement yield during the peak displacement.

The two most noticeable observations were the damage that occurred to the top of pile concrete and the lateral force degradation with repeated cycles. The damage to the top of the pile concrete was substantially greater than noted for previous specimens. While the column concrete was damaged, the concrete fill at the perimeter of CFST pile was also damaged as shown in Figures 3.40a) and b). During these cycles, the lateral strength of the column was also decreasing. The first cycle at 2.4% drift had force peaks of -1.4 to $1.4F_n$ (-91.4 to 93.8 kips), while the 6^{th} and last cycle had force peaks of -1.3 to $1.1F_n$ (-84.7 to 76.9 kips), both decreasing over $0.1F_n$ from the first cycle.

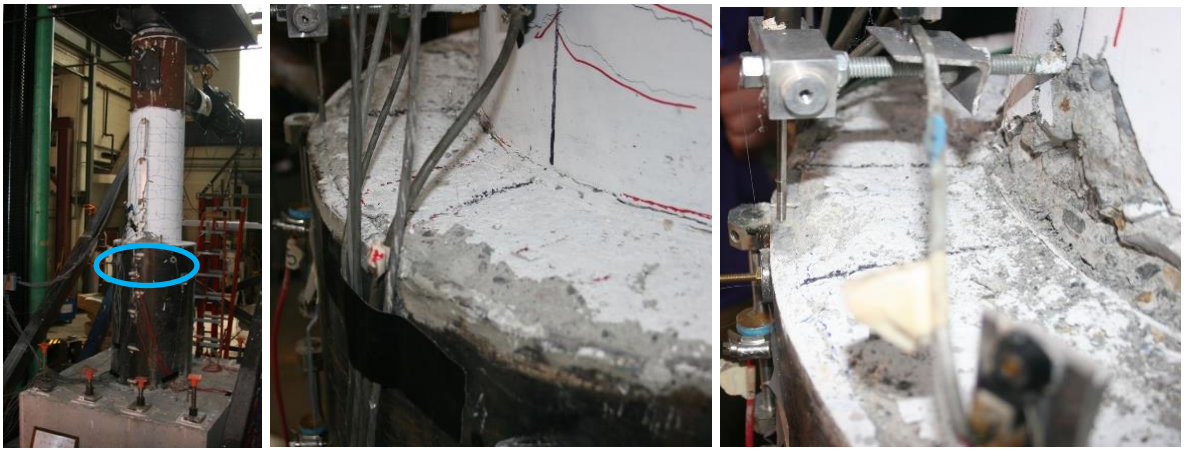

Figure 3.1. Specimen 30-21-LD a) Concrete Damage at the Edge of the Pile and b) Concrete Damage Near Base of the Column at 2.4% Drift

At drift displacements of 3.8%, the lateral load ranged from -1.4 to 1.4F_n (-93.7 to 92.9 kips), which was approximately equivalent to the previous first cycle at 2.4% drift. The cracks widened to a maximum width of 2.5 mm. The largest cracks were located on the northern and southern faces, both 0.3D_{COL} (6 in.) from the base of the column. The main observation during this cycle was the spalled region on the northern side increased greatly in area, as shown in Figure 3.41. Also, a small spalled area formed on the base of the southern face of the column.

Figure 3.41. Specimen 30-21-LD Northern Column Face Spalled Region at 3.8% Drift

Similar to the previous cycle, the strains measured at the peak displacement of this cycle, exceeded the yield strain for all N and S bar locations, except for the N bar and S bar locations -0.75D_{COL} as shown in Figure 3.42. The strains reached up to 0.024 in./in., which occurred on the N bar at 0.3D_{COL}.

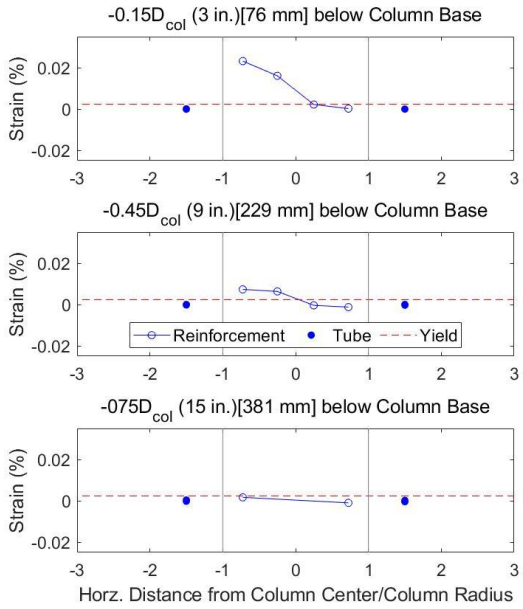

Figure 3.42. Specimen 30-21-LD Strain Distribution at 3.8% Drift

3.4.3 *Large Drift Cycles (Greater than 4.0% Drift)*

On the first cycle at 5.5% drift, the lateral load ranged from -1.5 to $1.3F_n$ (-98.9 to 90.0 kips), which was approximately equivalent to the previous cycle in tension and slightly less in compression. During this cycle, the maximum lateral force was reached of $-1.5F_n$ (98.9 kips). From this point on the lateral force would decrease slightly with each cycle in both compression and tension. The column base spalled region and crack increased in size, to a maximum width of 4.0 mm and exposed the transverse reinforcement on the southern face. The second cycle at 5.5% drift exposed the longitudinal reinforcement on the southern face as shown in Figure 3.43. The maximum crack width at this drift was 5.0 mm and the spalled region had increased greatly in area. For the remaining cycles, the cracks were too large to be measured, but they all continued to increase in size and quantity.

Figure 3.43. Specimen 30-21-LD Exposed Longitudinal Reinforcement at 5.5% Drift

The strains measured at the peak displacement for all the cycles at 5.5% drift all had the same pattern. The strains exceeded the yield strain for all N and S bar locations, except the N bar and S bar locations -0.75D_{COL}. The strains reached up to 0.06 in./in., which occurred on the S bar at -0.3D_{COL}. Figure 3.44 shows an example of the strain distribution at 5.5% drift.

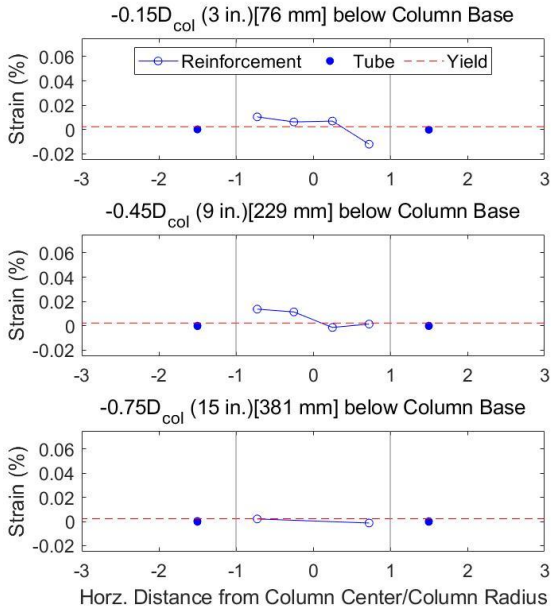

Figure 3.44. Specimen 30-21-LD Strain Distribution at 5.5% Drift

The third and fourth cycles at 5.5% drift, had a lateral load range of -1.4 to $1.2F_n$ (-92.8 to 79.0 kips), a decrease of $0.1F_n$ from the earlier cycles at 5.5% drift. There was increased damage to the pile concrete and exposed the longitudinal reinforcement on the northern face of the column. As mentioned before, the pile concrete damage was both the concrete at the edge of the tube, but also the concrete surrounding the column, which now had expanded to roughly 1 in. around the base of the column. The increased spalled area and pile concrete damage are shown in Figures 3.45 and 3.46.

Figure 3.45. Specimen 30-21-LD Increased Spalled Region at 5.5% Drift

Figure 3.2. Specimen 30-21-LD Top of Pile Concrete Damage at 5.5% Drift

During the fourth cycle, a crack on the southern side of the transfer block was noticed extending the entire height of the transfer block, shown in Figure 3.47. There was no noticeable change in the instrumentation or results before, during, or after this was noticed.

Figure 3.47. Specimen 30-21-LD Crack on Southern Side of Transfer Block

On the fifth cycle at 5.5% drift, the lateral load ranged from -1.3 to 1.1F_n (-87.3 to 76.3 kips) a decrease of 0.1F_n from the previous cycle. One of the longitudinal bars on the southern side of the column buckled slightly, as shown in Figure 3.48.

Figure 3.48. Specimen 30-21-LD Buckled Longitudinal Reinforcement on Southern Side of Concrete at 5.5% Drift

For the remaining five cycles at 5.5% drift, the lateral resistance of the column decreased around $0.03F_n$ (1-3 kips) per cycle, to a maximum resistance of $1.0F_n$ (66.8 kips) during the 10^{th} cycle at 5.5% drift or 19^{th} total cycle of the test. This was a decrease of $0.1F_n$ from the 5^{th} cycle at 5.5% drift. During these last five cycles at 5.5% drift, the bars on both the north and south sides of the column continued to buckle and the spalled area on both sides continued to increase in size. The state of the northern face of the column after the tenth cycle at 5.5% drift is shown in Figure 3.49..

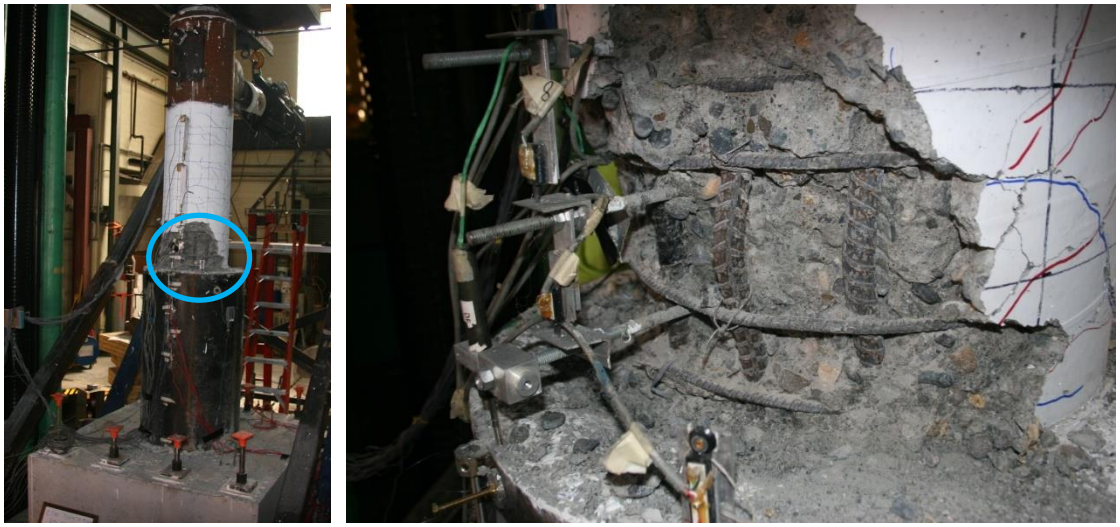

Figure 3.49. Specimen 30-21-LD Northern Face of Column after 10 cycles at 5.5% drift

Originally, the goal of this test was to test the specimen to failure with repeated cycles at 5.5% drift. However, the column was only losing a lateral strength of $0.03F_n$ per cycle, and therefore it was decided to run 2 cycles at a 6 in. displacement or a target drift of 9.72%.

On the first cycle at 8.3% to -9.4% drift, the lateral load ranged from -0.8 to $0.8F_n$ (-52.4 to 54.8 kips), a decrease of $0.2F_n$ from the last cycle at 5.5% drift. One of the longitudinal reinforcing bars on the Northside fractured in tension, which can be shown in Figure 3.50.

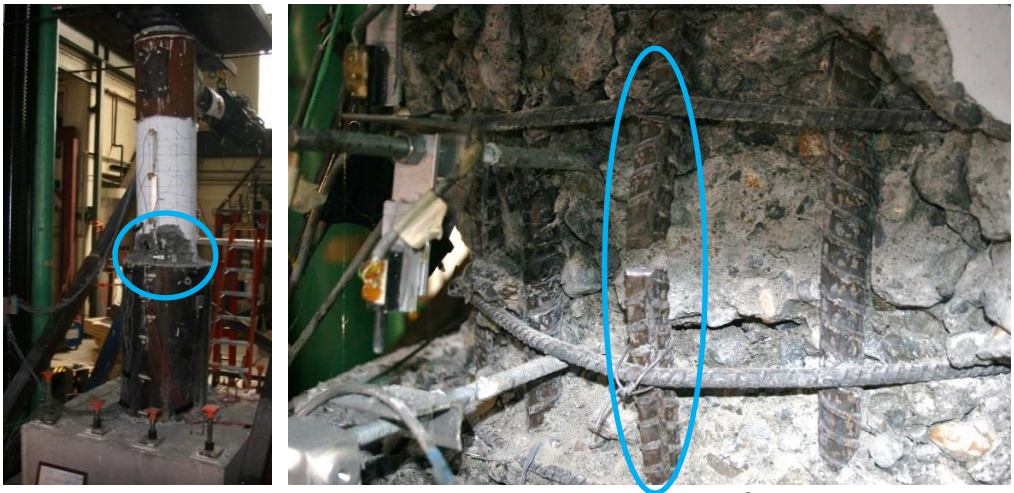

Figure 3.50. Specimen 30-21-LD Fractured Longitudinal Reinforcement on North side of Column at 9.4% drift

Loading was terminated after the second cycle when the column reached a drift of 9.9%. The last lateral load was $0.4F_n$ (27.1 kips), a decrease of $0.4F_n$ (27.7 kips) from the previous cycle. Another longitudinal reinforcing bar fractured during this cycle, this time on the southern side of the column, while all the remaining bars had completely buckled and the concrete at the base of the column had completely crushed. There was also widespread damage to the top of the pile concrete especially around the base of the column. The final state of the column can be shown in Figure 3.51.

Figure 3.51. Specimen 30-21-LD Final State of Column after 9.9% Drift

Throughout all load cycles, the pile showed no visible damage. There was no buckling or yielding of the pile, with the largest measured strain being 0.00017 in./in., which occurred 52 in. below the top of the tube, during the 5.5% drift cycles. There was no noticeable slip between the pile concrete in comparison to the edge of the tube at any point of the test. The measured slip on the outside of the tube had a maximum reading of 0.05 in. for the whole test. As shown in Figure 3.52, the top of the pile concrete appears heavily damaged on the edges and around the base of the column.

Figure 3.52. Top of Specimen 30-21-LD Pile with Column Removed

Chapter 4. NONLINEAR ANALYSIS

This chapter compares the experimental and simulated results of the four test specimens, which was done in in parallel with this experimental program [14]. By comparing the measured experimental results and the simulated results, the behavior of the connection, globally and locally, can be better understood and areas of weakness or concern can be analyzed and addressed.

As described in Section 2.1, Zhao modeled RC column to CFST pile connections in LS-Dyna, which were the basis for the design of the test matrix. The tested specimens had slight differences in their as-built material strengths, dimensions of the reinforcement layout, and geometry. Zhao revised his previous models with the as-built conditions to better simulate the actual geometry and material strengths used as a comparison with the experimental results. These comparisons are important, they are needed to validate and improve the FEA model used for these connections which will improve the accuracy of future modeling efforts.

The following sections show comparisons of the overall system behavior and specimen damage. Specifically, the comparison of the measured and simulated results investigates the similarities and differences in stiffness, degradation, strength, and deformability, and the comparisons of the damage, look at axial stress, compressive and tensile damage indicators, CDP and TDP respectively, for each specimen. Issues with the simulation results are also discussed.

The comparison of the overall specimen behavior is shown by plotting the force-drift hysteric curve of each specimen. The force is normalized by the nominal force, F_n, of each column, which are tabulated in Table 5.1. The comparison of the specimen damage is shown by comparing photos from the experimental testing with figures showing compressive or tensile damage from the FEA. For all simulated damage figures, the size of the concrete elements are 1.33 in., while the

drawn grid on the experimental specimens has a spacing of 5 in. The specimen test matrix is shown in Table 4.1 for additional reference.

Table 4.1. Specimen Test Matrix

Specimen Name	Tube Diameter (in.) [mm]	Tube Diameter/ Tube Thickness	Reinforcement Bar Size	Embedment Depth (in.) [mm]	Rib Size (in.) [mm]	Rib Embedment Depth (in.) [mm]
30-21*	30 [762]	60	#7	21 [533]	NA	NA
48-21	48 [1219]	96	#7	21 [533]	NA	NA
30-21-R	30 [762]	60	#7	21 [533]	2 [50.8]	2 [50.8]
30-21-LD	30 [762]	60	#7	21 [533]	NA	NA

*Specimen 30-21 is reference specimen

4.1 SPECIMEN 30-21

4.1.1 *System Behavior Comparison*

As shown in Figure 4.1, numerical simulation results closely match the measured experimental results. There are differences in the negative drift during the last few cycles. As stated before in Chapter 4, during these cycles the axial binding issue occurred which affected these cycles, and estimated values were substituted for these cycles.

- The initial stiffness and onset of lateral strength resistance degradation are well matched for both the measured and simulated results.
- There is a slight difference in the peak lateral strength, with the measured results reaching a peak strength of $1.4F_n$ at 2.5% drift, while the simulated results only reach a peak strength of $1.27F_n$ at 4.3% drift. Both results had similar ranges of drift, with the measured drift ranging from -8.1% to 7.8% drift, and the simulated drift ranging from -8.9% to 7.8%.

Another issue that occurred during these last cycles for the FEA was distortion in concrete components of the model, which did not allow for the final cycle at 8% drift to be completed.

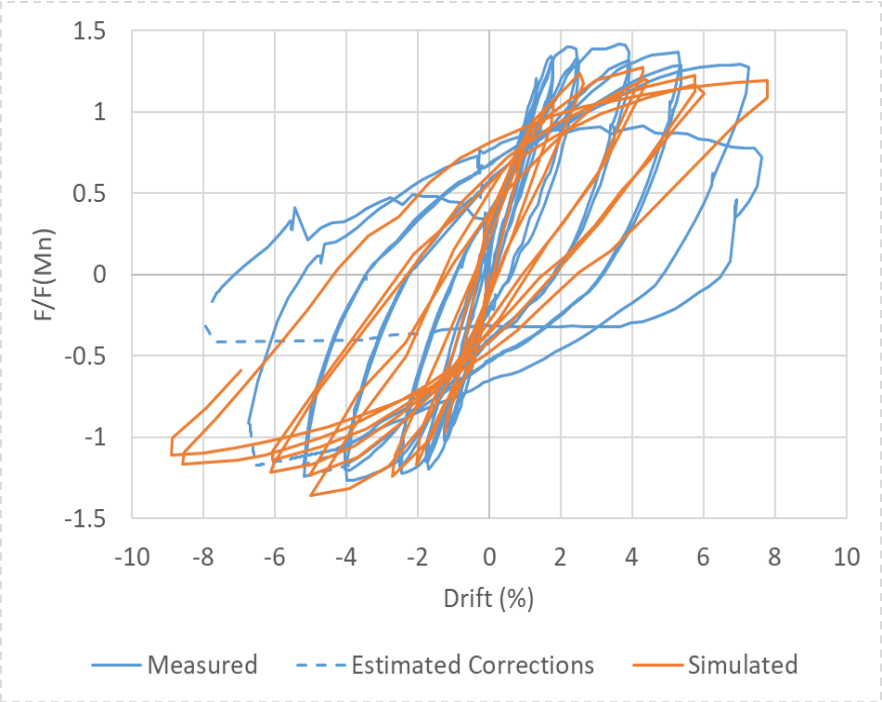

Figure 4.1. Specimen 30-21 Normalized by F_n Force-Drift Curve Comparison

4.1.2 *Damage Comparison*

At 2.2% drift, as shown in Figure 4.2a, the concrete spalled approximately up to 2 in. from the top of the pile.

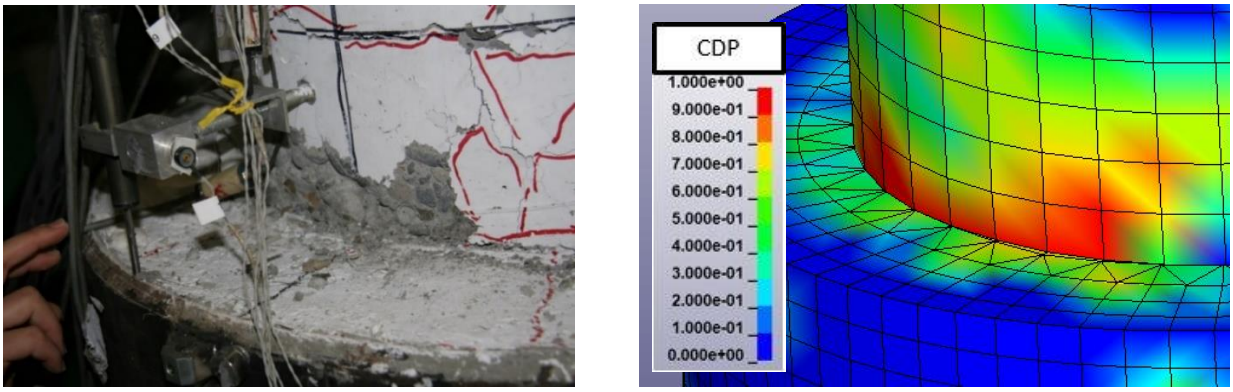

a) **b)**

Figure 4.2. Specimen 30-21 Compressive Damage at Base of Northern Column Face at 2.2% Drift: a) Observed and b) Simulated

Similar behavior is shown in Figure 4.2b with the red color representing the area of concrete that exceeded the normal strain of concrete indicating that region of the concrete has spalled. Also shown is the damage is concentrated at the base of the column, which is where the damage was focused in the experimental testing as well.

During the first cycle at 5.0% drift, as shown in Figure 4.3a, the spalled concrete area has increased in size, reaching up to 7 in. above the top of the pile.

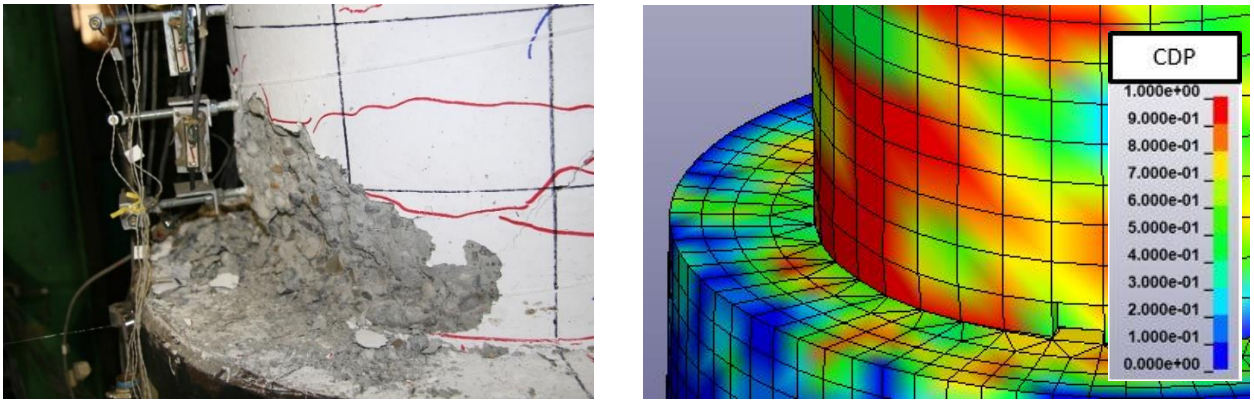

a) **b)**

Figure 4.3. Specimen 30-21 Compressive Damage at Base of Northern Column Face at 5.0% Drift: a) Observed and b) Simulated

The FEA damage, shown in Figure 4.3b, also shows an increased damaged area at the base of the column and the damage starting to spread to the concrete fill in the pile.

During the second to last cycle, which reached a drift of 7.0%, the concrete at the base of the column increased in spalled area furthering exposing both the longitudinal and transverse reinforcement as shown in Figure 4.4a.

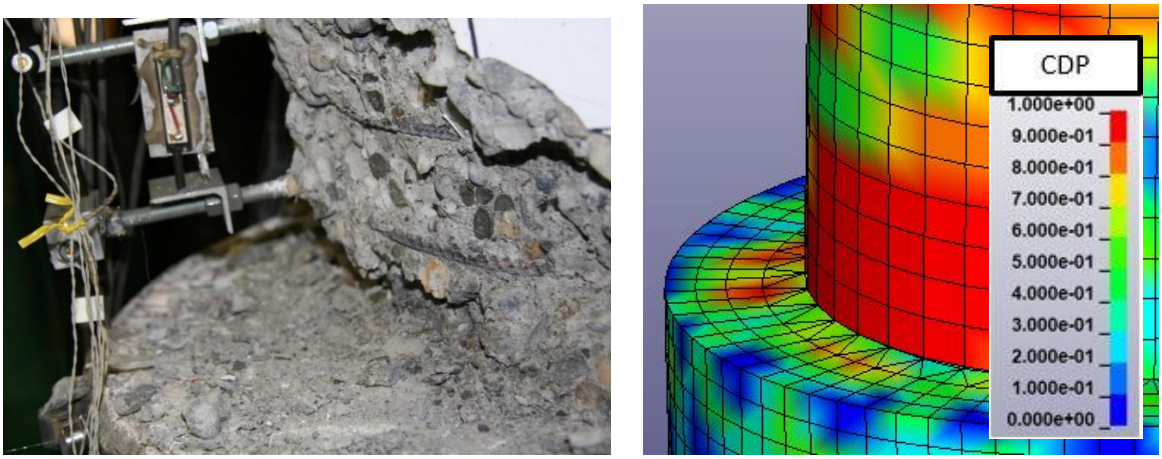

a) **b)**

Figure 4.4. Specimen 30-21 Exposed Longitudinal Reinforcement and Compressive Damage at Base of Northern Column Face at 7.0% Drift: a) Observed and b) Simulated

The FEA damage, shown in Figure 4.4b, shows the same area at the base of the column with increased damage, which would also lead to exposed reinforcement.

During the last cycle, which reached a drift of 8.0%, the concrete at the base of the column has completely spalled approximately 14 in. from the base of the column and the longitudinal reinforcement has buckled, as shown in Figure 4.5a.

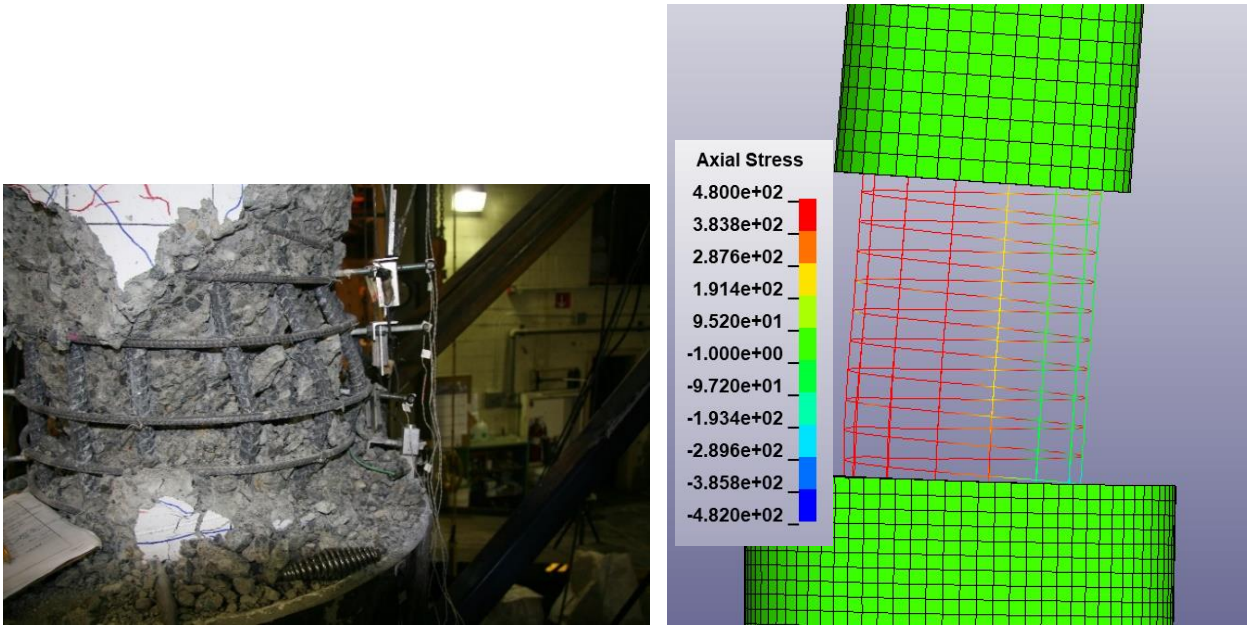

a) **b)**

Figure 4.5. Specimen 30-21 Buckled Reinforcement at Base of Southern Column Face at 8.0% Drift: a) Observed and b) Simulated Reinforcement Axial Stress

From the FEA axial stress, shown in Figure 4.5b, the southern longitudinal reinforcement is showing a compressive stress of 1 ksi, exemplifying that these bars have buckled since they are not taking any load.

4.2 SPECIMEN 48-21

4.2.1 *System Behavior Comparison*

As shown in Figure 4.6, the simulated response is similar to the measured results for Specimen 48-21 to the drift level of approximately 6%, with similar initial stiffness and no lateral strength resistance degradation as the drift level increases. There were issues with the model beyond 6% drift suggesting significant damage to the concrete between the reinforcement and tube, which was not seen in the test. As such, we will not compare the results beyond this drift level.

- There is a slight difference in the peak lateral strength, with the measured results reaching a peak strength of $1.33F_n$ at 2.8% drift, while the simulated results reach a peak strength of $1.41F_n$ at 3.7% drift.
- The measured and simulated results did not have similar ranges of drift, with the measured drift ranging from -9.4% to 9.0% drift, while the simulated drift ranged from -5.9% to 3.8%. This is due to the same issue that occurred for Specimen 30-21 where during the last cycles there was distortion in concrete components of the model, which again did not allow for the final cycles greater than 6% drift to be run.

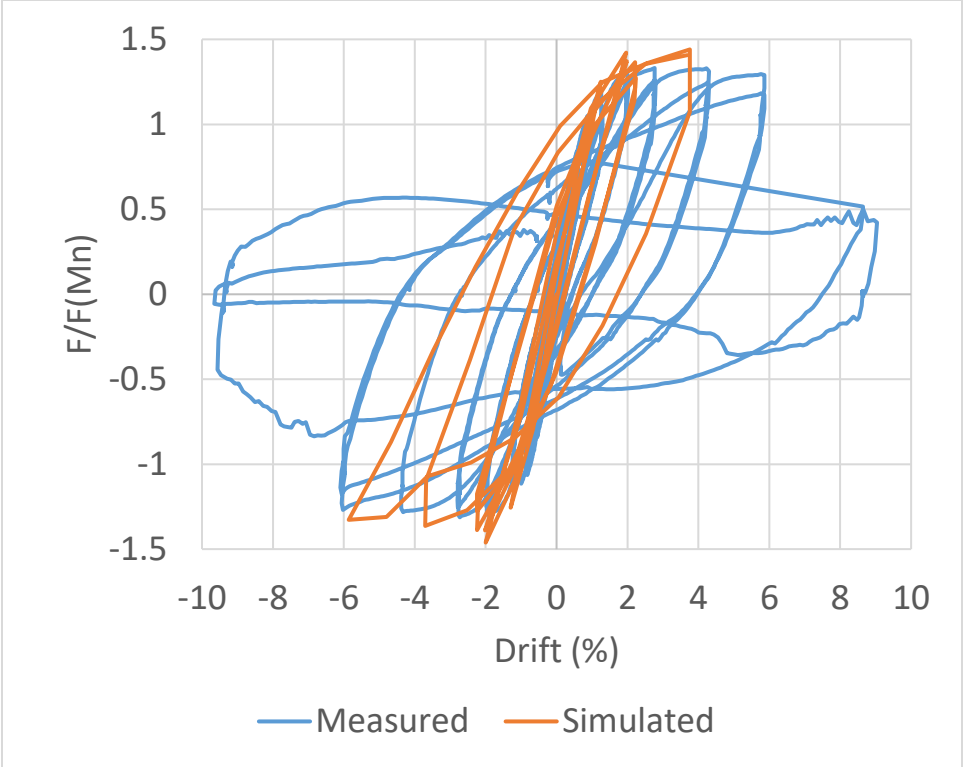

Figure 4.6. Specimen 48-21 Normalized by F_n Force-Drift Curve Comparison

4.2.2 *Damage Comparison*

At 1.1% drift, as shown in Figure 4.7, there is a radial crack on the top of the pile concrete, extending from the base of the column to the perimeter of the pile, as well as cracking around the base of the column.

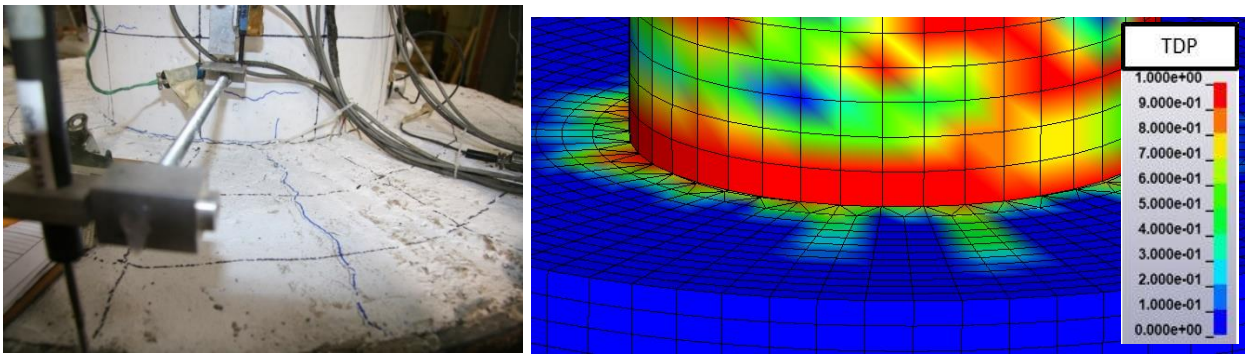

a) **b)**

Figure 4.7. Specimen 48-21 Radial Crack on Top of Pile Concrete at 1.1% Drift: a) Observed and b) Simulated Tensile Damage

As seen in Figure 4.7b, which is showing FEA tensile damage, there is significant damage around the base of the column as well as damage extending outward from the base. However, the damage to the top of the pile concrete does not extend out to the perimeter of the pile, as seen in Figure 4.7a.

At 2.6% drift, as shown in Figure 4.8a, there is spalling at the base of the column, reaching up to 6 in. above the column base.

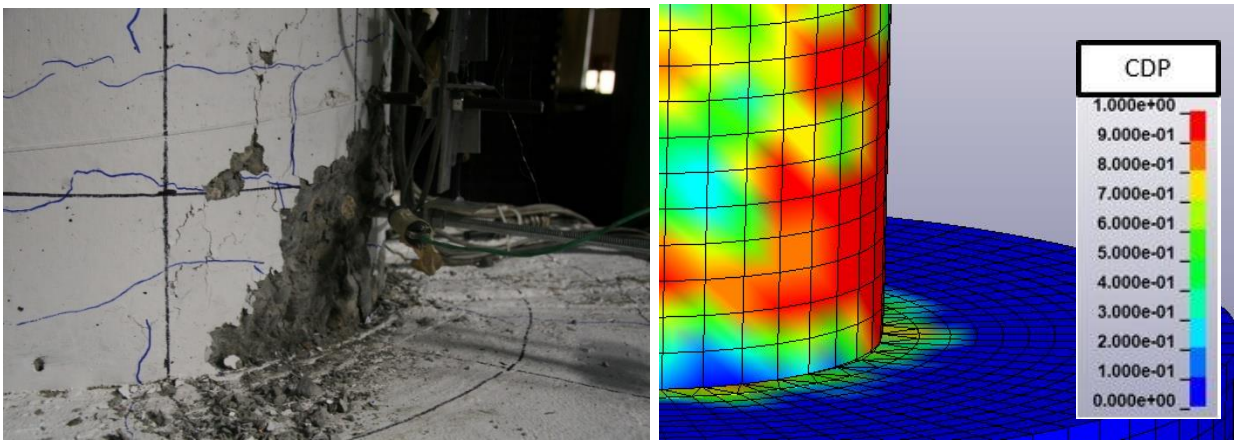

a) **b)**

Figure 4.8. Specimen 48-21 Compressive Damage at Base of Southern Column Face at 2.6% Drift: a) Observed and b) Simulated

Figure 4.8b shows there is also damage around the base of the column, which shows that the concrete has exceeded the normal strain of concrete indicating that region of the concrete has spalled. However, the damage seems to be more concentrated at the southern face of the column.

At 4.2% drift, as shown in Figure 4.9a, there is spalling at the base of the column, exposing both the longitudinal and transverse reinforcement.

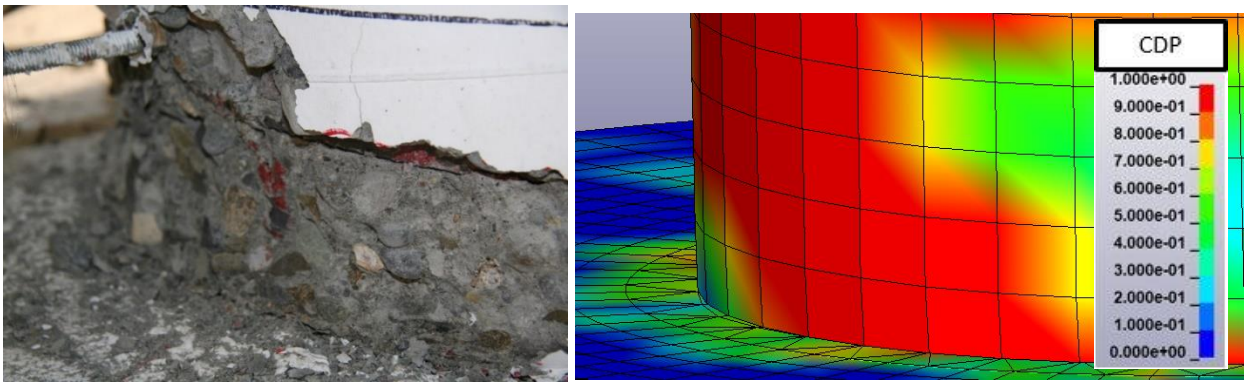

a) **b)**

Figure 4.9. Specimen 48-21 Exposed Reinforcement and Compressive Damage at Base of Northern Column Face at 4.2% Drift: a) Observed and b) Simulated

As shown in Figure 4.9b, there is compressive damage around the base of the column in the simulation, showing that the concrete has exceed the normal strain indicating that the region of concrete has spalled, which would also expose the reinforcement.

As seen in the overall system behavior results for Specimen 48-21, there was large distortion in the model elements at drift levels larger than 4.2%, as shown in Figure 4.10, and thus no damage figures were able to be compared at these drift levels.

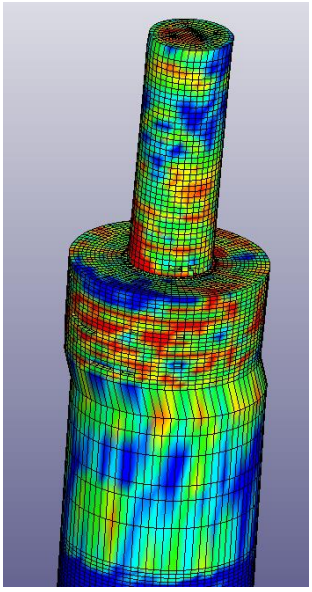

Figure 4.10. Specimen 48-21 Distorted Elements at 6.0% Drift

4.3 SPECIMEN 30-21-R

4.3.1 *System Behavior Comparison*

As shown in Figure 4.11, the simulated results closely follow the measured results for Specimen 30-21-R, with similar initial stiffness strength, cyclic response, and drifts corresponding to resistance degradation. The following summarized the results from the comparison:

- There is a larger difference in the peak lateral strength than compared to the other specimens, with the measured results reaching a peak strength of $1.36F_n$ at 4% drift, while the simulated results only reach a peak strength of $1.12F_n$ at 1.9% drift.
- Both results had similar ranges of drift, with the measured drift ranging from -9.7% to 8.9% drift, and the simulated drift ranging from -9.2% to 8.7%.
- The concrete distortion issues that occurred in the models of Specimens 30-21 and 48-21 were not observed in this model. This suggests that the distortion is exacerbated by the slippage of the concrete relative to the steel and this is mitigated by the embedded ring at the top of the pile, which helps mitigate the damage to the concrete in the pile.

There are two other key differences between the simulated and measured results. First, the simulated peak forces for cycles at 5.7% drift or smaller are slightly less than the measured results. Also, the test specimen sustained three cycles at 8.2% drift or greater before significant strength loss, while the simulated model sustained more than five cycles at similar drift levels and show no sign of lateral strength loss.

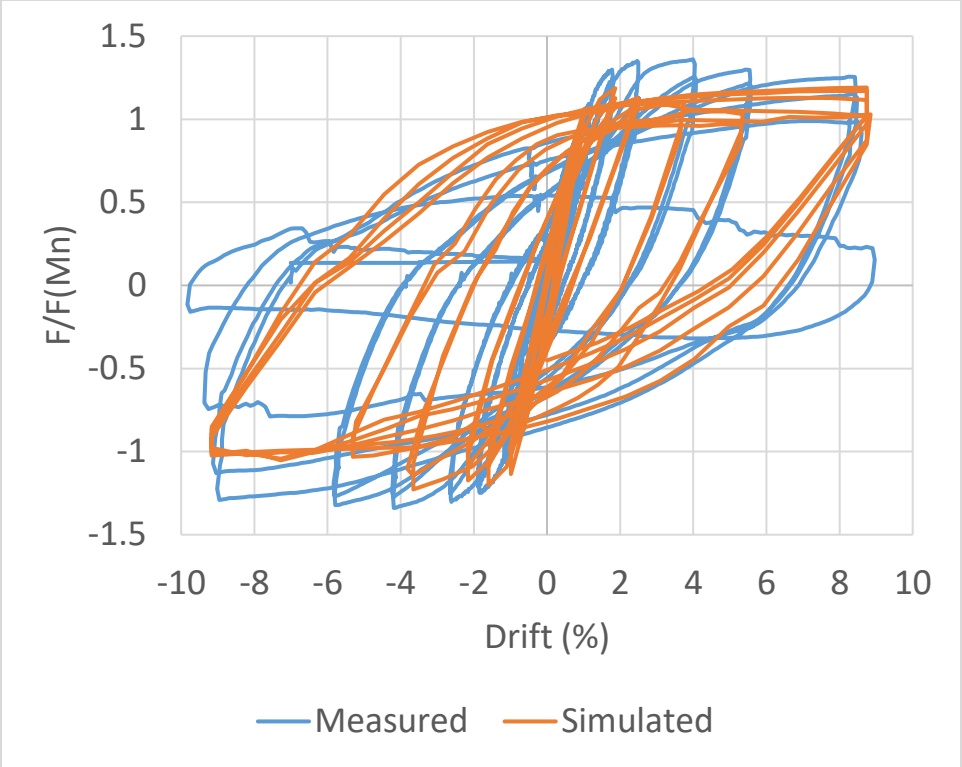

Figure 4.11. Specimen 30-21-R Normalized by F_n Force-Drift Curve Comparison

4.3.2 *Damage Comparison*

At 2.4% drift, as shown in Figure 4.12a, there is slight spalling at the northern base of the column, less than 2 in. from the top of the pile.

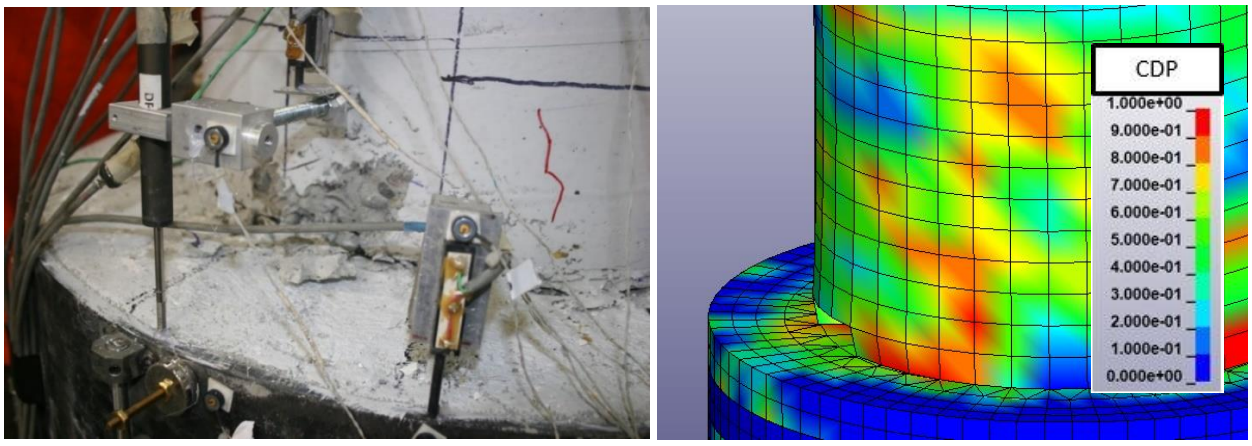

a) **b)**

Figure 4.12. Specimen 30-21-R Spalled Region and Compressive Damage at Base of North Face of Column at 2.4% Drift: a) Observed and b) Simulated

As shown in Figure 4.12b, the FEA compressive damage was also starting to occur at the northern base of the column.

At 5.5% drift, as shown in Figure 4.13a, there was significant spalling at the base of the column, approximately 7 in. up from the top of the pile, which exposed longitudinal and transverse reinforcement

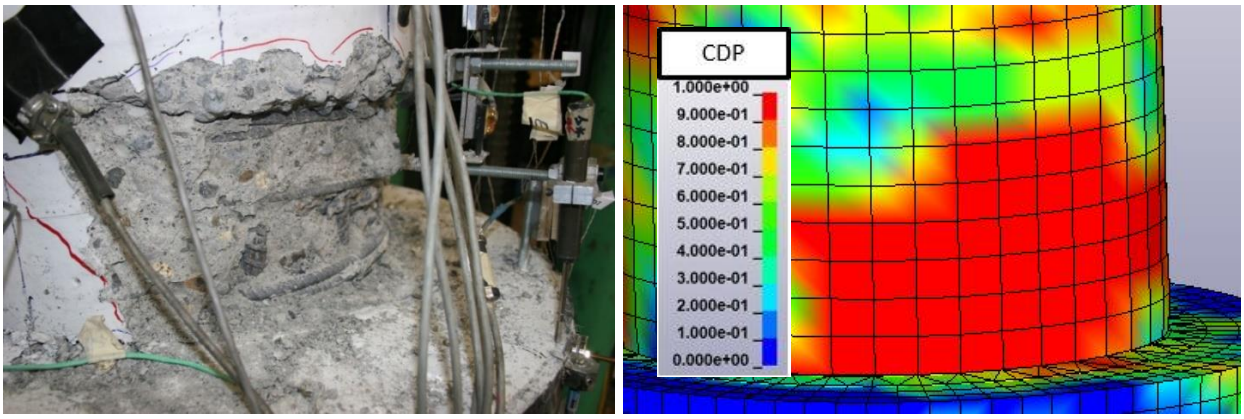

a) **b)**

Figure 4.13. Specimen 30-21-R Exposed Northern Longitudinal Reinforcement and Compressive Damage at 5.5% Drift: a) Observed and b) Simulated

The FEA compressive Damage, Figure 4.13b, shows a large damaged area at the northern base of the column, which would expose the reinforcement.

At 8.9% drift, the southern longitudinal reinforcement has buckled, shown in Figure 4.14a.

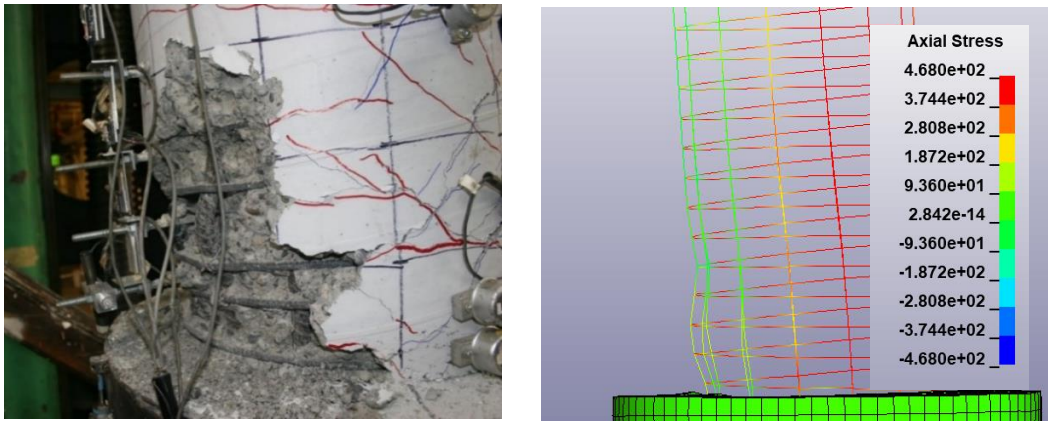

a) **b)**

Figure 4.14. Specimen 30-21-R Buckled Reinforcement at 8.9% Drift: a) Observed and b) Simulated Axial Reinforcement Stress

Figure 4.14b, showing the FEA axial stress, which shows the small axial stress in the southern longitudinal reinforcement and the buckled reinforcement as well.

4.4 SPECIMEN 30-21-LD

4.4.1 *System Behavior Comparison*

As shown in Figure 4.15, the simulated results closely follow the measured results with similar initial stiffness and slight lateral strength resistance degradation. There is a slight difference in the peak lateral strength, with the measured results reaching a peak strength of $1.33F_n$ at 2.5% drift, while the simulated results only reach a peak strength of $1.24F_n$ at 2.4% drift. The measured and simulated results did not have similar ranges of drift, with the measured drift ranging from -9.8% to 8.6% drift, while the simulated drift ranged from -5.3% to 5.2%. This is due to the same issue that occurred in the models of Specimens 30-21 and 48-21; those models have exhibited distortion in concrete components of the model. This distortion is due to increased concrete damage in the top of the pile, which is caused by the absence of the embedded rib and did not allow for the final cycles greater than 6% drift to be run.

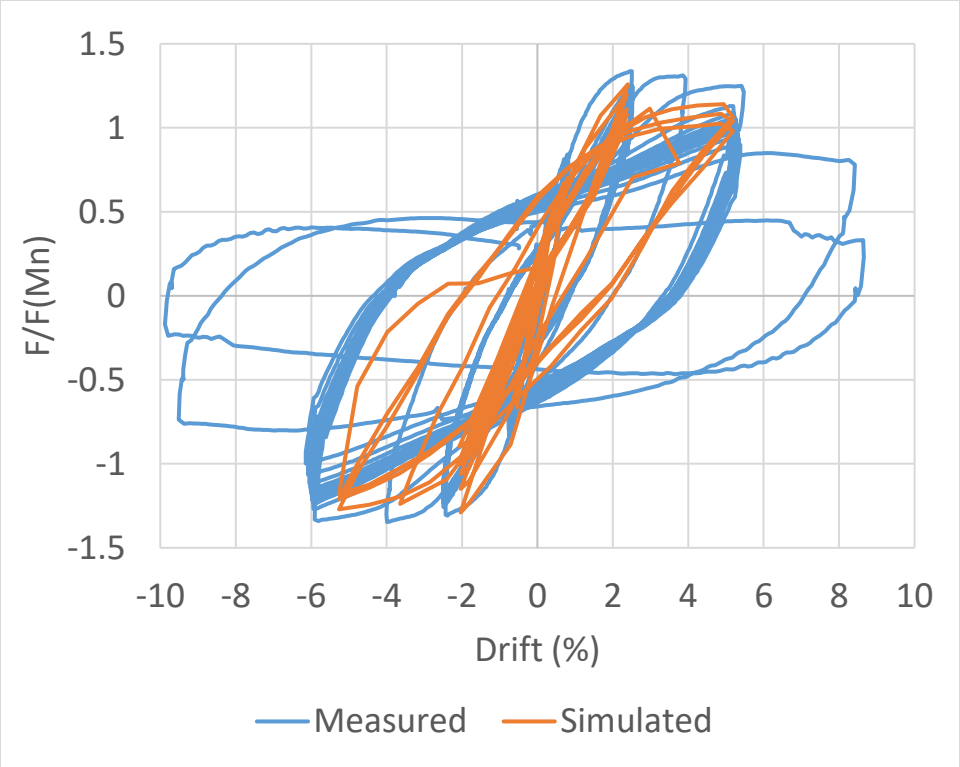

Figure 4.15. Specimen 30-21-LD Normalized by F_n Force-Drift Curve Comparison

4.4.2 *Damage Comparison*

At 2.4% drift, as shown in Figure 4.16a, the concrete is starting to spall on the northern base of the column.

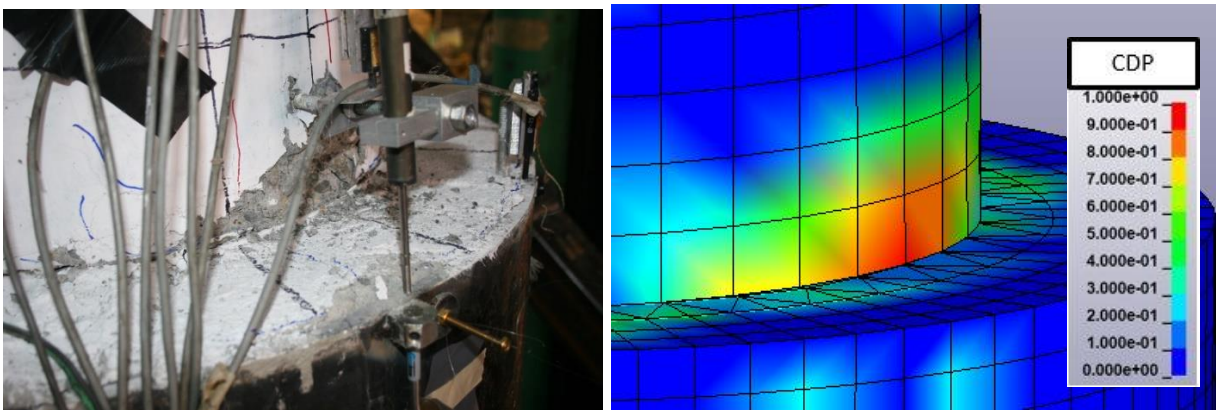

a) **b)**

Figure 4.16. Specimen 30-21-LD Initial Spall and Compressive Damage at Base of Northern Face of Column at 2.4% Drift a) Observed and b) Simulated

As shown in Figure 4.16b, the concrete has exceeded the normal strain of concrete indicating that region of the concrete has spalled and is concentrated at the northern base of the column.

At 5.5% drift, as shown in Figure 4.17a, spalling at the base of the column has increased over 7 in. above the base of the column and has exposed both the longitudinal and transverse reinforcement.

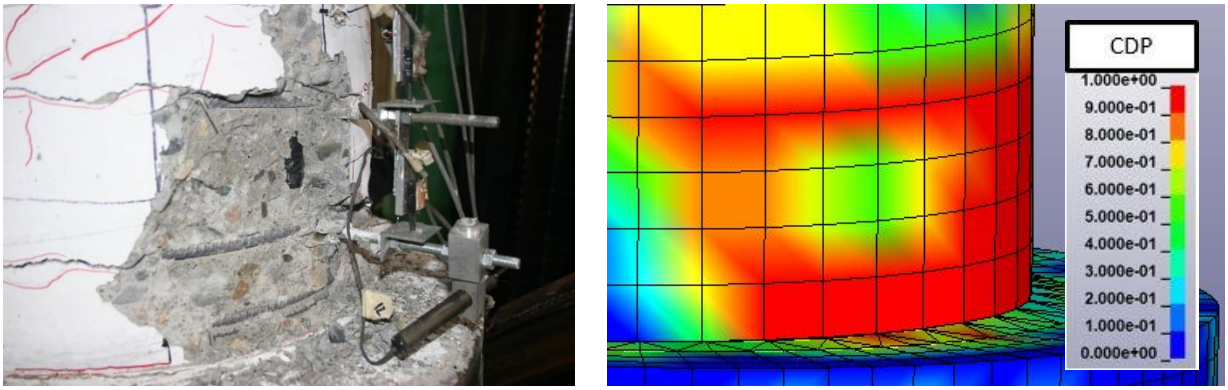

a) **b)**

Figure 4.17. Specimen 30-21-LD Exposed Longitudinal Reinforcement and Compressive Damage at 5.5% Drift: a) Observed and b) Simulated

As shown in Figure 4.17b, there is a large amount of FEA compressive damage in the same region, which would expose the reinforcement.

As seen in the overall system behavior results for Specimen 30-21-LD, there was large distortion in the model elements at drift levels larger than 5.5% and thus no damage figures were able to be compared at these drift levels.

4.5 COMPARISON SUMMARY

In terms of overall behavior, the simulated and measured results are similar in terms of strength and stiffness. However, in most cases, the simulated model began to lose strength before the measured specimens did. In addition there is information about the response of the connection from the simulated models that cannot be seen in the experimental tests. Lateral degradation is

evident in the simulated results for Specimens 30-21 and 30-21-LD, while there is no significant lateral strength degradation in the simulated results for Specimens 48-21, and 30-21-R. The measured peak strengths of each specimen are within $0.1F_n$ of the simulated peak strengths, except Specimen 30-21-R's results, which were $0.24F_n$ apart. The simulated results' drift ranges were similar for Specimens 30-21 and 30-21-R, however, the drift ranges for Specimens 48-21 and 30-21-LD were very different.

In terms of specimen damage, the observed damage from the experimental testing matched the simulated damage from the FEA results for all specimens. The photos from the experimental testing showing the onset, spread, and regions of concrete spalling around the column base closely matched the damage figures from the FEA model. The buckled reinforcement at large drift levels was seen both in the damage photos and the axial stress figures. While not shown for all specimens and drift levels, the tensile damage results from the FEA showed similar results to the cracking that occurred to the concrete fill in the pile.

The main issue between the model and the test specimen is the concrete element distortion for all the specimens without the embedded rib in the pile at large displacements. The element distortion issue is the result of high demands on the concrete for Specimens 30-21, 48-21, and 30-21-LD. As seen in both the measured and simulated results, specimens with an embedded rib are able to reach higher strengths and larger drift levels, all while not experiencing lateral strength degradation. This is also seen in the damage comparison figures, with the damage not being able to be compared at these large drift levels. There is also significantly less damage to the concrete at the top of the pile, as seen in there is no distortion in the concrete elements for the simulated results and reduced damage to the test specimen with the embedded ring, 30-21-R.

Chapter 5. SUMMARY AND CONCLUSIONS

This summary and conclusions will utilizes results from the prior research report and this research study to draw broader conclusions and recommendations.

5.1 SUMMARY OF RESEARCH

This research has evaluated a new direct RC pier column to CFST pile connections. The connevtions were developed for use in accelerated construction of high-speed rail and other transportation systems in seismic regions. Four half-scale connections were tested to failure under cyclic inelastic deformation. The data was analyzed and evaluated. Nonlinear analyses of these four specimens were completed with the LSDyna computer program, and the analytical predictions were compared to the measured and observed performance in experiments. The combined results of these studies were analyzed design recommendations are proposed.

The study addressed several parameters with respect to this direct pier to pile connection including:

- Pile diameter to column diameter ratio. This study used 20-inch diameter columns. Both 30 in. diameter pile and a 48 in. diameter piles were tested.
- Supplemental Bond. One specimen included a supplemental rib at the top of the steel tube inside the pile.
- The inelastic response of the connection under long-duration cyclic loading to simulate subduction zone motion.

5.2 OBSERVATIONS FROM THE EXPERIMENTAL RESEARCH

While testing, the following observations were made:

- Yielding of the column reinforcement occurred during smaller cycles of approximately 0.6% column drift
- Spalling that exposed the column transverse reinforcement occurred during moderate cycles between 3.7% to 5.5% column drift
- Spalling that exposed the column longitudinal reinforcement occurred during moderate cycles between 4.1% to 5.5% column drift
- Extensive buckling of the column reinforcement occurred during larger cycles ranging 7.5% to 8.8% drift for all specimens not tested under long duration loading
- Specimen 30-21-LD experienced buckling at 5.2% drift due to its different displacement history
- Specimen 30-21-LD was the only specimen that had a longitudinal reinforcing bar fracture during testing, with both a bar on the north and south sides of the column fracturing during the last cycle
- All tests were terminated due to lateral strength resistance loss caused by bar buckling and concrete crushing during large drift cycles between 8.1% to 9.9% column drift
- Specimen 30-21-R was the only specimen able to withstand four cycles at 9% or greater drift before significant lateral strength loss
- Specimens 30-21 and 30-21-LD experienced significantly more damage, radial cracks, and concrete spalling, to the top of pile concrete than the other two specimens. Specimen 48-21 did have radial cracks on the top of the pile concrete, while Specimen 30-21-R did not show any damage

When comparing the overall specimen behavior of each specimen, the following observations were made:

- The flexural strength of all of the columns were 32% to 40% larger than the predicted
- Specimens 48-21 and 30-21-R were able to maintain lateral strength after the peak lateral resistance was reached at approximately 4.0% column drift for both, while Specimen 30-21 and 30-21-LD showed lateral strength degradation after the peak lateral resistance was reached, which occurred at 3.7% and 6% column drift respectively
- Specimens 30-21, 30-21-R, and 30-21-LD sustained one cycle at 8% drift, while Specimen 48-21 did not sustain any cycles at 8% drift or greater

When comparing the experimental results to the LSDyna nonlinear FEA model results, the following observations were made:

- The FEA system behavior of all specimens generally matched the measured experimental system behavior
- The simulated results for Specimens 30-21 and 30-21-LD showed lateral strength degradation after peak strength was reached
- The models of Specimens 30-21, 48-21, and 30-21-LD failed due to distortion in the concrete component of the model: the drift capacity of the models were less than the tests
- Specimen 30-21-R did not show any distortion in the concrete component of the model suggesting that it is the right connection design with the uncertainties in the field with respect to concrete strength and field placement including eccentricity
- The damage from the FEA closely resembled the damage from the experimental behavior in terms of concrete spall, cracking, and buckling of reinforcement

5.3 CONCLUSIONS AND RECOMMENDATIONS

The following conclusions and recommendations were reached based on interpretation of experimental observations, measured response, and comparison to FEA:

- Composite action between the column and the CFST pile occurs at approximately 15 in. below the column base
- Without the addition of an embedded rib inside the pile, a 48 in. pile connection showed better overall performance than a 30 in. pile connection, both in terms of strength degradation, deformation capacity, specimen damage, and slip between the steel tube and the connection concrete. However, it is not possible to investigate the internal damage in any of these specimens. The model indications substantial internal damage to the connection I the specimens without the supplemental rib.
- With the addition of an embedded rib inside the pile, the connection showed improved performance with both an increase in strength and ductility, a decrease in the slip between the connection concrete and the steel tube, and a decrease in damage
- When testing the connection under long-duration cyclic loading, the connection was able to sustain lateral resistance for multiple cycles at large drift levels
- The results of the FEA model provided a good representation of the measured behavior.
- Using CFST piles, in a direct column to pile connection, offers a an economical and practical alternative for accelerated bridge construction.

REFERENCES

[1] American Association of State Highway and Transportation Officials. (2017). *AASHTO LRFD Bridge Design Specifications*. American Association of State Highway and Transportation Officials (AASHTO), Washington, DC.

[2] American Association of State Highway and Transportation Officials. (2015*). Guide Specifications for LRFD Seismic Bridge Design with 2012, 2014 and 2015 Interim Revisions*. American Association of State Highway and Transportation Officials (AASHTO), Washington, DC.

[3] American Concrete Institute. (2014). *Building Code Requirements for Structural Concrete (ACI 318-14)*. Farmington Hills, MI.

[4] California Department of Transportation (Caltrans). (2019). *Seismic Design Criteria*. Sacramento, CA

[5] Chang, M. (2021). *Seismic Performance of Column-to-Drilled-Shaft Connections in Reinforced Concrete Bridges,* Thesis, University of Washington.

[6] Kappes, L., Berry, M., and Stephens, J. (2013). *Performance of Steel Pipe Pile-to-Concrete Cap Connections Subjected to Seismic or High Transverse Loading,* Technical Report FHWA/MT-13-001/8203, Montana Department of Transportation.

[7] Kortum, Z. (2021). *Impacts of Cascadia Subduction Zone M9 Earthquakes on Bridges in Washington State: SDOF Idealized Bridges,* Thesis, University of Washington.

[8] Liu, Y. (2012). *Lateral Behavior of Reinforced Concrete Columns Supported on Type II Shafts,* M.S., University of California, San Diego.

[9] Mehraein, M. (2016). *Seismic Performance of Bridge Column-Pile-Shaft Pin Connections for Application in Accelerated Bridge Construction,* Dissertation, University of Nevada, Reno.

[10] Stephens, M. T. (2016). *Design Expressions and Dynamic Evaluation of CFST Bridges Subjected to Seismic Hazards,* Dissertation, University of Washington.

[11] Tran, H. V. (2015). *Drilled Shaft Socket Connections for Precast Columns in Seismic Regions,* Dissertation, University of Washington.

[12] Washington State Department of Transportation (WSDOT). (2020). *Bridge Design Manual (LRFD) M 23-50*. Olympia, WA.

[13] Yeutter, A. S. (2020). *A RC Slab to CFT Column Connection for Improved Seismic Behavior of Multi-Story Buildings,* Thesis, University of Washington.

[14] Zhao, M., Lehman, D., and Roeder, C. (2021). *Analytical Investigation of a New Direct Column-to-Cased Shaft Connection,* Engineering Structures, 245 (October 2021)

APPENDIX 1 –SPECIMEN DRAWINGS

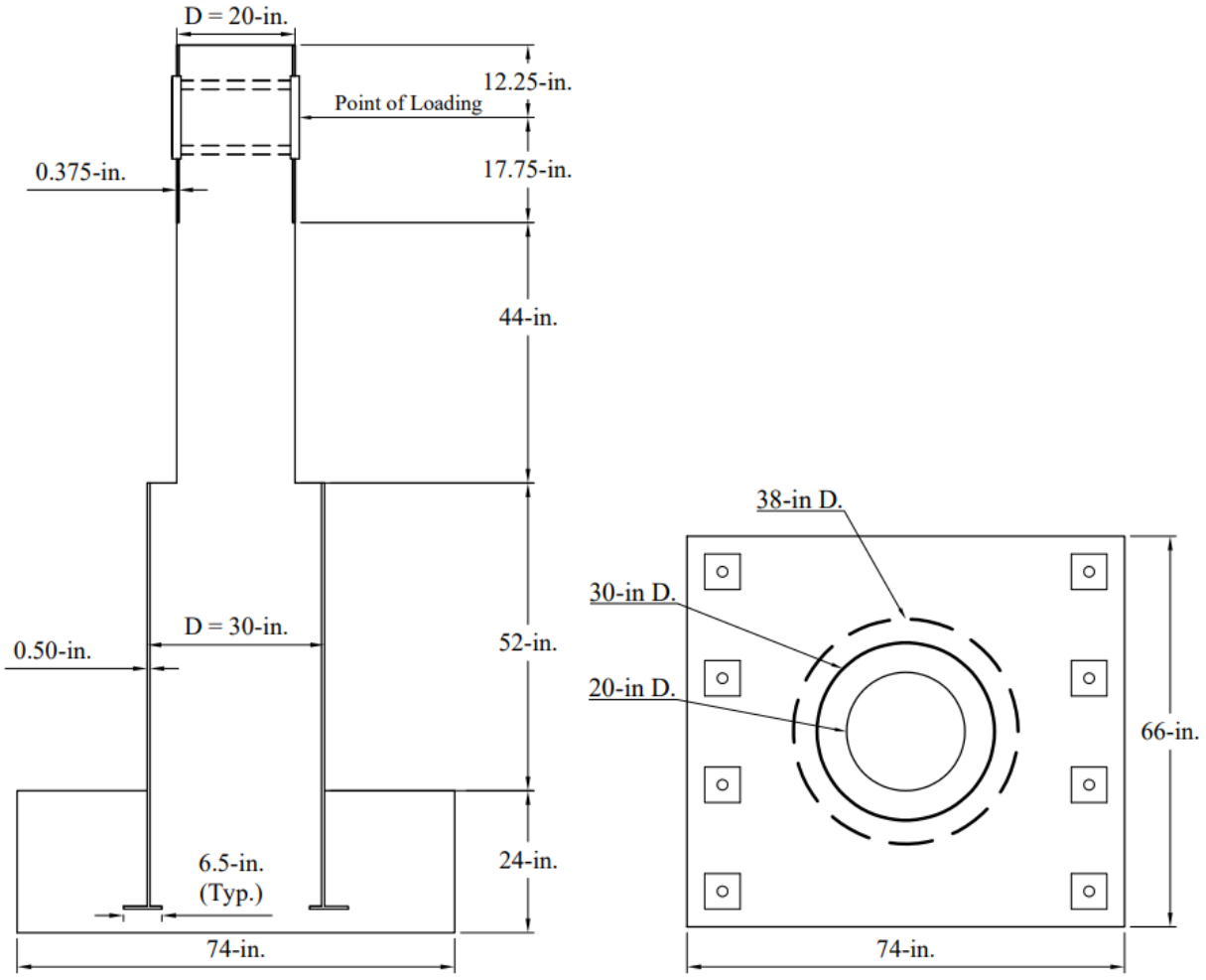

Figure A1.1 Specimen 30-21 and 30-21-LD Dimensions

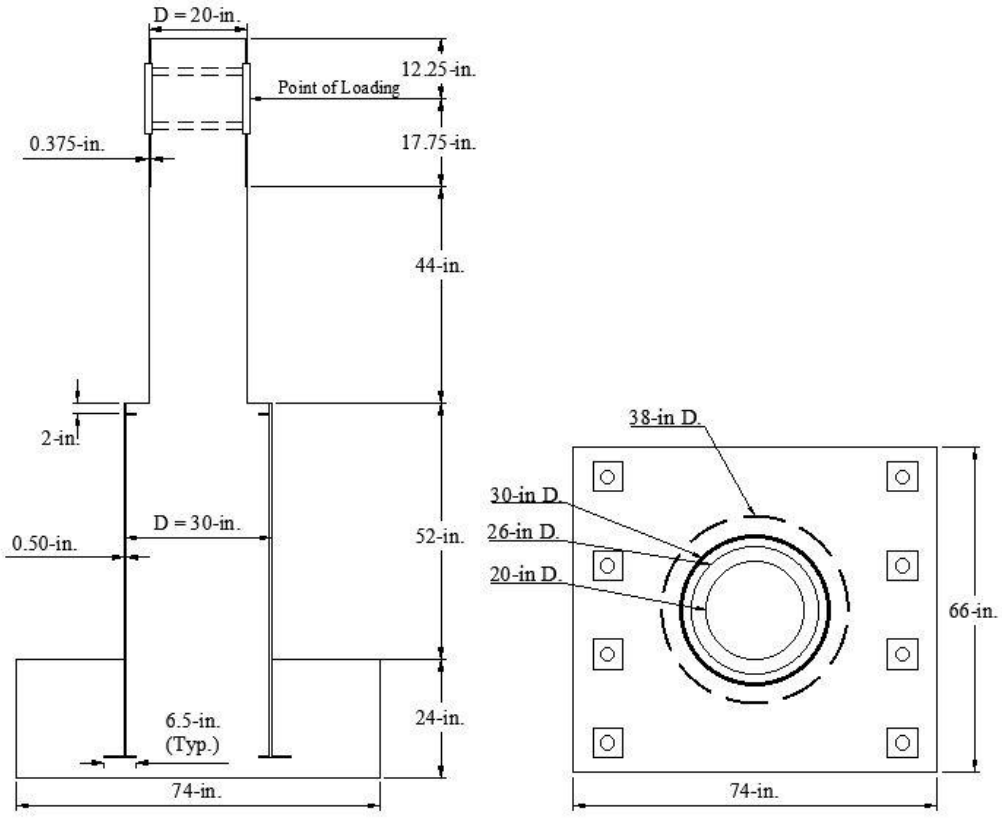

Figure A1.2 Specimen 30-21-R Dimensions

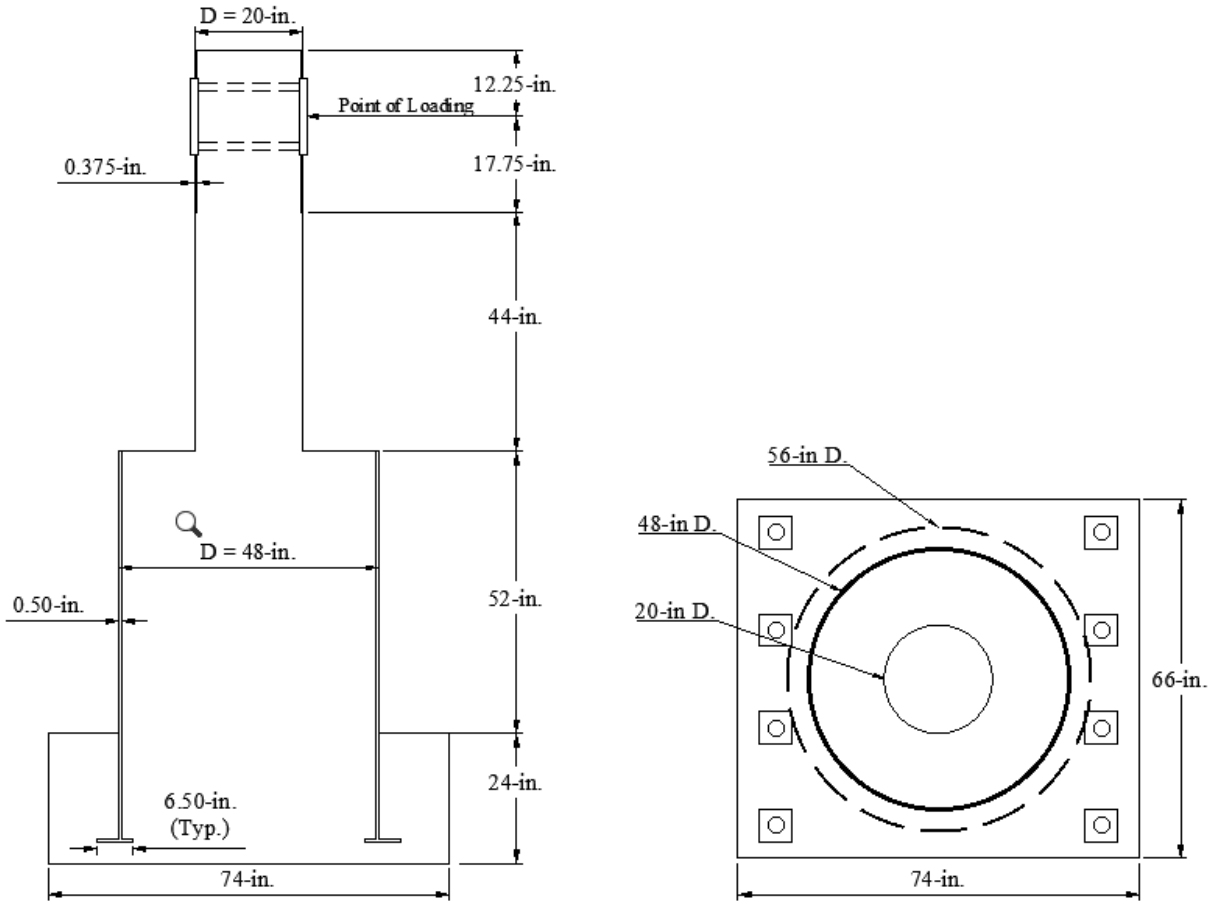

Figure A1.3 Specimen 48-21 Dimensions

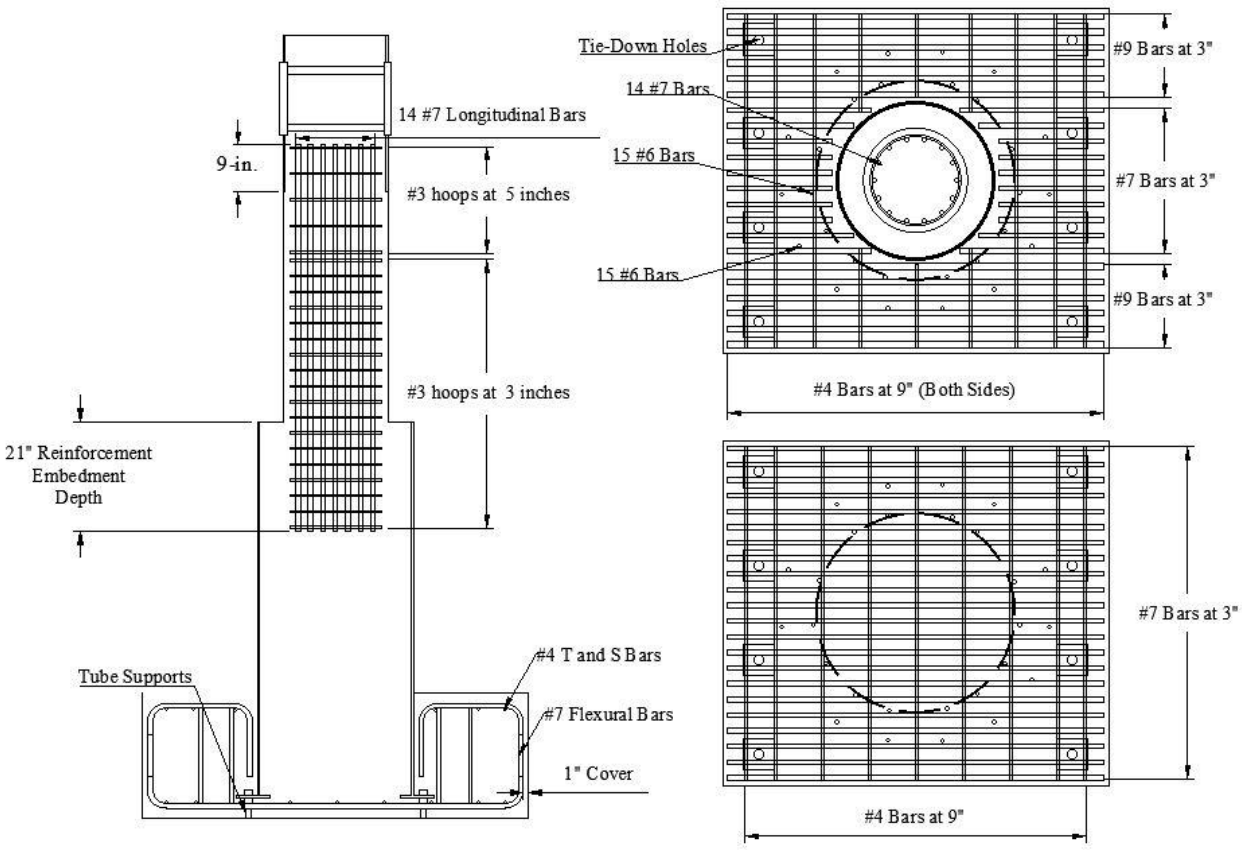

Figure A1.4 Specimen 30-21 and 30-21-LD Reinforcement Layout

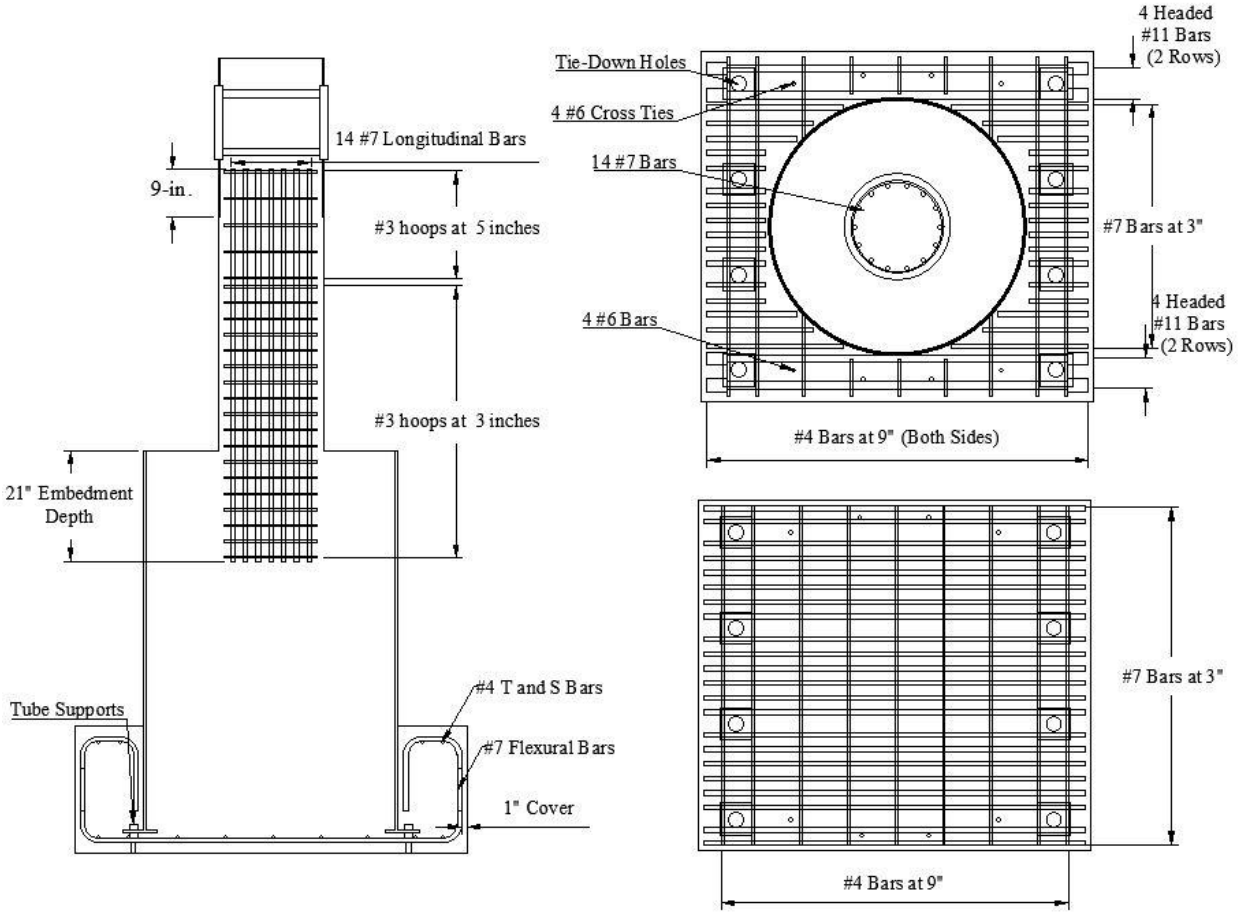

Figure A1.6 Specimen 48-21 Reinforcement Layout